PART 1

Nanomaterials and Nanotechnologies

1

Carbon-based Nanomaterials

Fullerenes, carbon nanotubes (CNTs), nanodiamonds (NDs) and carbon quantum dots (CQDs) are nothing new, and were discovered long before the year 2000; these discoveries were followed, in 2005, by that of graphene. Due to their remarkable physico-chemical properties, fullerenes, CNTs and graphene have given rise to innumerable applications, and their use has progressed continually; nevertheless, the use of graphene has increased much faster than that of fullerenes and CNTs (Figure 1.1).

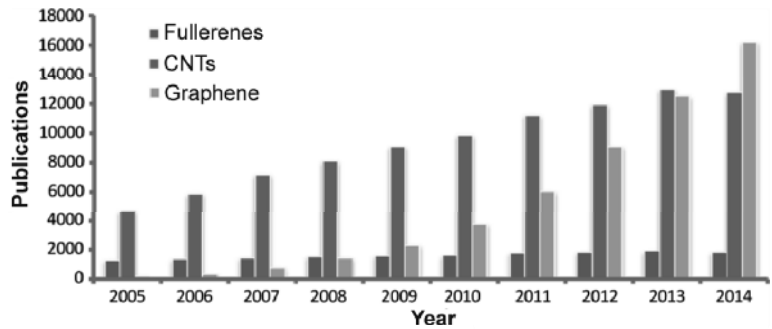

Figure 1.1. *Number of publications on the subject of fullerenes, CNTs and graphene from 2005 to 2014. Based on [LI 15]*

The number of publications concerning these three families of compounds between 2005 and 2014 clearly shows an "explosion" in the number of articles on the subject of graphene; over the course of 7 years, from 2007 to 2014, this went

For a color version of all the figures in this chapter, see: www.iste.co.uk/lacaze/nanotechnology.zip.

from around 50 to over 16000, exceeding scientific production on the subject of CNT, discovered a whole decade earlier than graphene.

Moreover, the implication of Asian countries (notably China, South Korea and Japan) in this research is notable, representing more than 50% of total publications between 2005 and 2014 (China alone accounts for 36% of production); the United States accounts for just over 22%, and the rest of the world for 27%.

1.1. Fullerenes

Since Kroto *et al.*'s [KRO 85] discovery of buckminsterfullerene C_{60} (henceforth C_{60} fullerene) in 1985, where they demonstrated that it had a balloon-like structure made up of an assembly of sp^2 carbon atoms arranged in the form of pentagons (12) and hexagons (20), a whole area of chemistry has developed in connection with fullerenes; a whole host of applications have also emerged in biology, medicine, electronics and energy.

Following on from C_{60} and C_{70}, the two most stable and widespread forms (Figure 1.2), new fullerenes with higher carbon numbers have subsequently been synthesized.

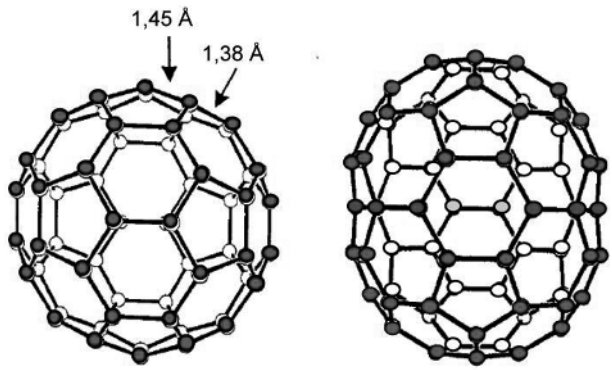

Figure 1.2. *Fullerenes: C_{60} (a) and C_{70} (b)*

COMMENT ON FIGURE 1.2.– *a) The C_{60} fullerene consists of an assembly of 10 pentagonal and 20 hexagonal carbon rings. The red and white symbols represent the C atoms in the foreground and background of the projection plane. b) The structure of the C_{70} fullerene is equivalent to that of two C_{60} hemispheres joined by*

10 C atoms (six shown in dark blue, four in light blue, two of which cannot be seen) at the midplane of the molecule. Adapted from [BAL 98a].

The stability of these fullerenes results from the arrangement of hexagons and pentagons. The IPR (Isolated Pentagon Rule) notably states that a fullerene, with a given number n of carbon atoms, will be stable if each pentagon is surrounded by hexagons and has no contact with another pentagon. In the case of the C_{60} fullerene, there are 1812 geometric isomers of which only one (with symmetry I_h) verifies the IPR. The energy difference between the most stable (noted 1) and the least stable (noted 1812) isomers in the series is of the order of 540 kcal/mol [SUR 17]. This energy largely results from the tension exerted by the curvature of the bonds.

1.1.1. *Properties of fullerenes*

Given their cage-like carbon structure, featuring only covalent bonds between sp^2 carbons, fullerenes are naturally hydrophobic and therefore insoluble in aqueous media. In order to use fullerenes for biological purposes, transformations must be carried out to make them more hydrophilic; this is achieved by grafting hydroxylated groups (COOH or OH), corresponding to exo-functionalization reactions, notably onto C_{60} and a number of other fullerenes (C_{70}, C_{80}, etc.) which are produced on a commercial scale. However, these latter fullerenes are expensive due to the difficulties inherent in large-scale production.

The presence of a cavity suggests that it might be possible to encapsulate chemical species. This is of interest with regard to the design of various markers, such as those used in medical imaging. The encapsulation of metals would result in a whole new category of nanomaterials, corresponding to the formation of endometallofullerenes (EMF), whose stability is a function of the fullerene and the small number of metal atoms encapsulated within the cage. The electrophilic character of fullerenes and their strong electronic affinity also mean that they are strong electron receivers, and are sometimes considered as “electron sinks”.

1.1.1.1. *Electrophilic and antioxidant properties of fullerenes*

The electrophilic character of fullerenes was established as early as the 1990s. This discovery suggested the possibility of forming anions with six negative charges, corresponding to the acceptance of six electrons by the LUMOs (lowest unoccupied molecular orbitals) of the fullerene. This hypothesis was confirmed by the existence of potassium salts (K_6C_{60}) in crystalline form.

More evidently still, the progressive six-step electrochemical reduction of C_{60} and C_{70} demonstrates the possibility of obtaining six stable reduction states of fullerene [XIE 92] (Figure 1.3).

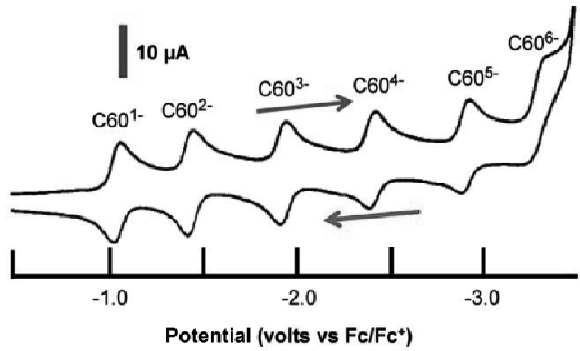

Figure 1.3. *Voltametric curves showing redox of C_{60} in a low temperature acetonitrile/toluene solution (–10°C)*

COMMENT ON FIGURE 1.3.– *The reduction curve obtained by a potential sweep from 0 to –3.5 V (blue arrow) shows six distinct reduction peaks, each corresponding to the gain of an electron. The reverse oxidation curve (red arrow) is clearly defined and also shows six oxidation peaks, corresponding to the six successive anionic states; this proves the stability and reversibility of these six redox states. Sweep speed: 100 mV/s. Potentials given against the ferrocene/ferricenium$^+$ (Fc/Fc^+) redox couple. Adapted from [XIE 92].*

The electronic affinity of fullerenes means that they can be used as electron carriers in photovoltaic cells, achieving energy yields of the order of 10% (see section 4.1). Fullerenes also have numerous applications in the biomedical field. C_{60} and its derivatives, in combination with various hydrophilic groups with relevant biological properties, have been used in cancer and AIDS therapies (anti-retroviral therapy against HIV-1). Functionalized by carbohydrate chains, fullerenes have also proven to be good antibacterial agents. Their high affinity for radicals, which results from radical addition on the numerous double bonds of the fullerene, effectively makes them act as "sponges" for these radicals. As powerful antioxidants, fullerenes are used in biology to neutralize radical oxygen species (ROS) such as the $O_2^{\bullet -}$ superoxide ion, $HO^{\bullet}$ hydroxyls, and hydrogen peroxide, H_2O_2, which are particularly damaging to DNA and certain proteins. They are also used in "niche" cosmetic products, including creams based on liposoluble C_{60} fullerenes, marketed as antioxidants, with a power comparable to, or better than, that of vitamin E-based products [ACQ 17]. All these properties, used in a medical context, have been described in well-documented papers [BAK 07, LAL 13, CAS 17].

1.1.1.2. *Chemical reactivity and exo-functionalization*

As fullerenes are considered to be electrophilic reagents, a whole chemistry of functionalization, corresponding to nucleophilic or radical additions or even cycloaddition reactions of the Diels-Alder and Prato type[1], can be envisaged. This has been described in detail by Taylor and Walton [TAY 93], and more recently by Georgakylas *et al.* [GEO 15] in the case of C_{60} and C_{70}.

Among fullerene derivatives, the fullerenols and carboxyfullerenes obtained by grafting hydroxyl or carboxyl groups onto the surface of fullerenes present an advantage in comparison with simple fullerenes in that they are soluble in aqueous and biological media. This is the case of hexacarboxylated fullerenes (carboxyfullerenes), which are fullerenes carrying three pairs of carboxylic acids, comprising a mixture of two stereoisomers, C3-C_{60} and D3-C_{60} (Figure 1.4)[2].

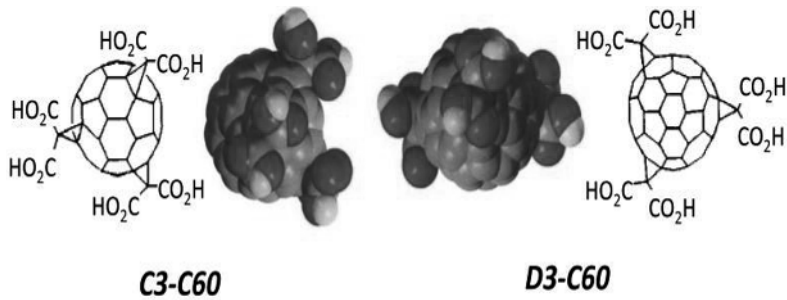

Figure 1.4. *Structure of two carboxyfullerene stereoisomers, C3-C_{60} and D3-C_{60}. Based on [DUG 97]*

Like simple fullerenes – but with the advantage of aqueous solubility – these derivatives have strong antioxidant properties; they notably have the capacity to destroy the peroxide ion $O_2^{\bullet -}$, a toxic subproduct of cell metabolism. This property makes them excellent neuroprotectors, and research in this area is still ongoing [DUG 97, ALI 04, GHA 05, YE 15b].

1 The Prato reaction is a cycloaddition of a nitrogen ylide to an ethylenic double bond, resulting in an (R)N-pyrrolidine or, in the case of fullerenes, an (R)-pyrrolidino fullerene. The nitrogen ylide is obtained *in situ* by the action of formaldehyde on an amino acid ($RNH\text{-}CH_2\text{-}COOH + CH_2O \rightarrow H_2C = N^+(R)\text{–}CH_2^- + CO_2 + H_2O$).

2 These C3-C_{60} and D3-C_{60} isomers, obtained by reacting ethyl 2-bromo malonate with C_{60} in the presence of NaH, differ in that they belong to symmetry groups C3 and D3.

1.1.1.3. *Endometallofullerenes*

The idea that the interior of the fullerene "cage" to trap atoms came hot on the heels of the discovery of fullerenes themselves. As early as 1985, Heath *et al.* [HEA 85] identified the first fullerene made up of 60 carbon atoms and containing a lanthanum atom[3] using mass spectrometry. A few years later, the same authors isolated several metallofullerenes with 60, 70, 74 and 82 carbon atoms, the last of which, $La@C_{82}$[4], is the only one which is stable in contact with air [CHA 91].

One remarkable feature of these new compounds is that the metal is not released when the compound is placed in a biological medium; this constitutes a considerable advance in comparison with classic metal chelates. This stability probably results from an electron transfer between the La atom and the fullerene, creating a $La^{3+}@C_{82}^{3-}$ ion pair, and presumably also to the fact that the mesh of the fullerene is small enough to prevent the La^{3+} ion from diffusing outward.

This discovery, which opened promising perspectives in the medical field (notably for diagnostic and therapeutic applications) resulted in an almost immediate upsurge in research into synthesizing new EMF, some of which are useful in the field of oncology. For instance, the gadolinium fullerenol $Gd@C_{82}(OH)_{22}$, initially used as a contrast agent in nuclear magnetic resonance imaging (MRI), has also been shown to have strong anti-cancer properties, different from those of simple fullerenes; furthermore, it retains low cytotoxicity [KAN 14][5].

1.1.1.4. *Endocluster fullerenes*

This new family of metallofullerenes was isolated for the first time in 1999 by Dorn and coworkers [STE 99]; as before, these molecules are obtained by producing an electrical discharge between graphite electrodes, containing a metal oxide[6], in a

3 The lanthanum fullerene was synthesized by laser ablation of a disk of graphite impregnated with lanthanum salts ($La Cl_3$).

4 The notation $La@C_{60}$ indicates that the lanthanum ion is contained inside the cage formed by the fullerene.

5 The gadolinium ion (Gd^{3+}), used as a contrast agent in MRI, is unfortunately extremely toxic. This toxicity is greatly reduced when the Gd is encased in a hydrophilic modified fullerene, i.e. one which is soluble in biological media. A commercial product made by Bayer, Magnevist®, corresponds to the EMF C_{60} gadolinium EMF $(Gd@C_{60}[C(COOH_yNa_{1-y})_2]_{10}$ into which a $[C(COOH_yNa_{1-y})_2]_{10}$ chain is grafted [LAU 07].

6 The most widespread method consists of using the electrical arc discharge to vaporize graphite. Other methods based on laser ablation, radiofrequency heating or heating using a resistor in an oven, ion implantation through the cage or opening the cage to insert ions have also been used to synthesize ECFs.

reactor. The difference here lies in the inclusion of a small quantity of dinitrogen in the reactor (Figure 1.5).

The remarkable result of this reaction is that it produces a new type of fullerene in which a cluster corresponding to a trimetallic nitride is embedded. The most abundant endocluster fullerenes (ECF) of this family is obtained using scandium. It has the formula $Sc_3N@C_{80}$ and consists of an 80-atom cage, into which scandium nitride with a symmetrical plane structure is inserted. A detailed description of the various functionalization reactions carried out on the surface of the cage of metallocluster fullerenes, which sometimes present higher levels of reactivity compared to simple fullerenes, can be found in a number of recent articles [GOO 17, YAN 17, BAO 18].

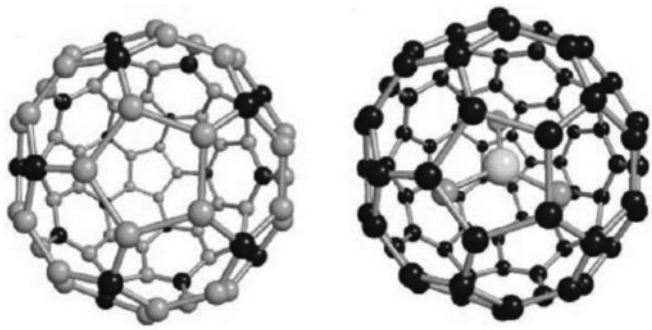

a) b)

Figure 1.5. *Structure of the C_{80} fullerene and of the ECF $Sc_3N@C_{80}$. a) C_{80} fullerene (symmetry Ih, symmetry axis of order 5) showing a 5 C ring (light blue) surrounded by five rings of 6 C atoms (dark blue). b) Structure of the $Sc_3N@C_{80}$ endocluster fullerene. Based on [STE 99]*

An additional family of EMF has been developed by replacing nitride clusters with clusters of metal dicarbides of the form M_2C_{2n}, which can exist in the form $M_2C_2@C_{2n-2}$. Depending on the atomic volume of the metal, the size of the fullerene cages can vary from 72 to 88 carbon atoms (in the case of scandium) and from 90 to 104 atoms (lanthanum). More recently still, a series of "giant" fullerenes has been discovered involving yttrium carbide clusters: the size of the cages in this case can be up to 130 carbon atoms. The formula for these clusters is Y_2C_{2n} where 2n is from 92 to 130 inclusive [PAN 18].

All these compounds have immense potential applications, but the fact that they are currently obtained in only very small quantities (a few tens of mg) and in the

form of mixtures, requiring painstaking separation using preparative chromatography, obviously limits their practical use. In contrast with simple fullerenes (C_{60} and C_{70}) and their exo-functionalized derivatives, which have already been subject to extensive research in connection with biomedical applications [CAS 17], ECF and EMF are generally studied in the context of fundamental research, aimed at better understanding the behavior of clusters of a small number of atoms, confined in a constrained space and interacting with carbon atoms.

1.1.1.5. *Onion-like fullerenes*

Onion-like fullerenes (OLFs) are a family of multi-shell fullerenes consisting of a concentric, nested assembly of multiple fullerenes of no more than around 10 nm. Various methods are used to create OLFs; the most common approach involves heat annealing, a powder made up of carbon nanodiamonds (NDs; see section 1.2) to produce large quantities of these OLFs [ZEI 16] (Figure 1.6).

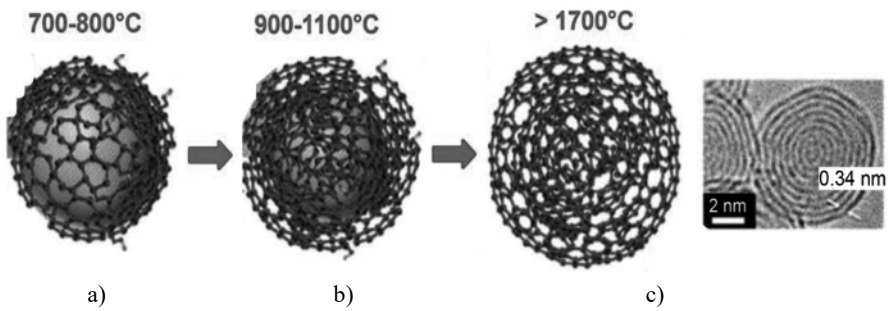

Figure 1.6. *Progressive transformation of nanodiamonds (ND) into OLF. a) Beginnings of the formation of a fullerene structure at 700–800°C on the surface of the ND. b) Formation of multiple concentric layers of fullerenes at 900–1100°C. c) Terminal phase in obtaining an OLF at T > 1700°C and the corresponding TEM image, showing multiple concentric carbon layers. Adapted from [ZEI 16]*

The transformation of NDs (which are commercially available) into OLFs essentially consists of a gradual change from sp^3 to sp^2 carbons. This transformation, which takes place in vacuum or in the presence of inert gases, starts to take place at temperatures around 1300°C and is completed at temperatures of up to 1800–2000°C. Under these conditions, we obtain OLFs which are homogeneous in size, about 5 nm in diameter, but in agglomerated form. Stable solutions can be obtained after disaggregation and an acid treatment, and these solutions are used in manufacturing conductive inks [VAN 17].

These compounds have electrical conduction properties far superior to those of activated carbon[7] and are thus highly valuable for creating supercapacitors with extremely fast response times [PEC 10]. They are eminently suited for use as power devices for energy storage, notably in the realization of pseudo-supercapacitors (see Chapter 3), combining a high charge/discharge speed with larger amounts of stored energy than those found in simple supercapacitors [VAN 17]. A very large number of alternative preparation techniques, which do not use NDs, may be used; these involve degrading various low-cost carbon products, and this makes them more economically competitive in relation to activated carbon [ZEI 16].

1.2. Carbon nanodiamonds

Although NDs were first discovered in the 1960s[8], they were not widely used until the late 1990s, once a detonation-based production technique had been firmly established [GRE 88]. These nanomaterials are now produced on a commercial scale, and are used both for improving the mechanical properties of plastics and for diagnosis and treatment in the field of medicine.

1.2.1. *Principal techniques used in creating nanodiamonds*

Owing to growing awareness of their importance, many different techniques have been developed for producing NDs. The most widespread approaches currently include detonation in a closed chamber, laser ablation and grinding using diamond microcrystal microbeads at high temperature and high pressure [MOC 12]. Their size is between 4 and 5 nm. Nanodiamonds can also be produced using CVD (chemical vapor deposition) techniques, in the form of films of varying thicknesses, between 20 nm and 5 µm [BUT 08]. The detonation method consists of introducing a mixture of two explosive compounds, such as the trinitrate derivatives trinitrotoluene (TNT-$C_7N_3O_6H_5$), trinitrobenzene (TNB-$C_6N_3O_6H_3$) or hexogen

7 Activated carbon (or activated charcoal) is a variety of porous carbon, available in the form of micronic powder or granules. It is obtained by pyrolyzing waste natural products, such as olive pulp, making it a particularly cheap product. Its high porosity and very high molecular adsorption power make it ideal for liquid filtering and gas purification operations; it is also an ideal substance for electrodes used in constructing supercapacitors.

8 First discovered by Danilenko *et al.* [DAN 04b] in 1963 but ignored by the scientific community, NDs were synthesized for the second time in 1982 by another Russian team, in the context of research aimed at synthesizing diamonds using detonations in a constrained space. Diamond-containing soots were initially considered as an insignificant subproduct; they finally began to attract attention once the possibilities for functionalization became apparent, and as potential uses in the biomedical sphere began to come to light.

($C_3N_6O_6H_6$), which do not release oxygen on explosion, into a closed metal chamber. The reaction takes place in a humid atmosphere of nitrogen and carbon dioxide (Figure 1.7).

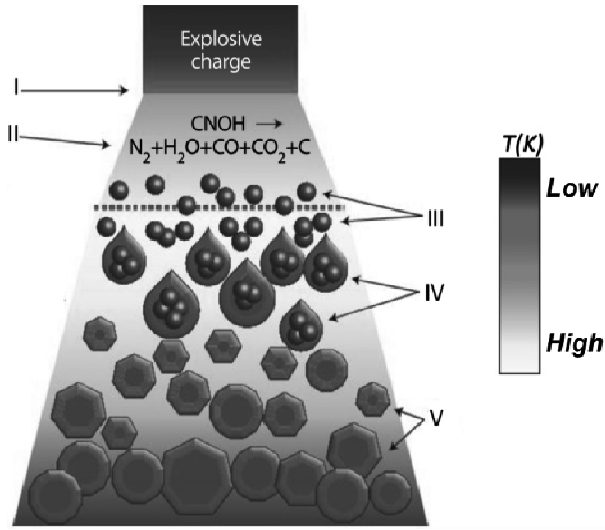

Figure 1.7. *Simplified diagram showing the detonation technique for nanodiamond production*

COMMENT ON FIGURE 1.7.– *I) Front of the shockwave resulting from the explosion. II) Products resulting from the explosion of a combination of TNT/TNB. III) Region in which the temperature (from 2200 to 4500 K) and pressure (from 13.5 to 16.5 GPa, i.e., approximately 150000 atmospheres) correspond to the formation of carbon clusters. IV) Coagulation of clusters in the form of nanodroplets. V) Crystallization, growth and agglomeration of NDs. Adapted from [MOC 12].*

As soon as the explosion occurs, the temperature and pressure immediately increase, establishing within a confined space the conditions needed for carbon nanoclusters to form. These nanoclusters become ND (in soot form) on reaching the coldest parts of the reactor [DAN 05]. The soot formed after the explosion of the charge may contain up to 75% ND, ranging from 4 to 5 nm in size; the remainder is made up of graphitic carbon (between 25% and 75% by weight, depending on the conditions), metals and oxides (between 1% and 8 % by weight), and nitrogenous

derivatives. The yield in terms of carbon-based products is around 4%–10% of the mass of the explosive charge[9].

Nanoparticles (NPs) are essentially composed of sp^3 carbons, but they may also be partially covered by layers of graphitic carbon (sp^2) on the surface, or functionalized by various chemical groups resulting from reactions with dangling bonds on the surface.

1.2.2. *Key properties of nanodiamonds*

From a mechanical perspective, the properties of NDs are very similar to those of pure diamonds. They are characterized by extreme hardness and a very high Young elasticity modulus, making them ideal for use in polishing hard surfaces such as ceramics. Their high level of chemical stability means that they can also be used in very hostile environments.

Fluorescence and biocompatibility are two further interesting properties, opening the way for biomedical applications in both diagnostics and treatment, due to the ease of surface functionalization.

1.2.2.1. *Fluorescent nanodiamonds*

Fluorescent nanodiamonds (FNDs) are a new family of nanomaterials, ranging in size from 35 to 100 nm [HSI 16] and characterized by the presence of a structural defect inside the crystal (Figure 1.8a) [CHA 08].

This defect, named NV, corresponds to a coupling between a vacancy V (absence of a carbon atom) and a nitrogen atom N, adjacent to the vacancy. It can be created easily by irradiating ND crystallites with a beam of helium (He^+) ions [CHA 08] or protons (H^+)[10]. Nanodiamonds treated in this way (equivalent to n-doped NDs) emit

9 Raman spectrometry may be used to identify the main functional groups found on the surface of NDs. The core of the ND is characterized by a high-intensity peak centered at 1328 cm^{-1}; this is characteristic of sp^3 carbons. The presence of graphitic carbons, sp^2, along with that of oxygenated functional groups resulting from oxidation on contact with air is shown by the presence of a wide spectral band located between 1500 and 1800 cm^{-1}; this results from the addition of the graphitic carbon band, centered at 1590 cm^{-1}, a band due to the vibration of the angular deformation of OH at 1640 cm^{-1}, and a plateau resulting from the presence of carboxyl groups between 1740 and 1760 cm^{-1}.

10 The sub-micrometer diamond powders used to make FNDs are obtained at high temperature and high pressure, and contain about 100 ppm of impurities in the form of nitrogen atoms dispersed throughout the diamond structure. Under the effect of ion

stable red fluorescence when stimulated by a laser. The intensity of the fluorescence is a function of the concentration of NV, which increases as the energy of the He^+ ion beam used to create the defect is strong (NV concentration may vary between 10 and 30 ppm in relation to the number of carbon atoms; in the absence of treatment, their concentration is lower than 1 ppm)[11]. The biocompatibility and high stability of FNDs, along with their non-toxic nature and high-intensity red fluorescence, make them ideal for use in the biomedical sphere; they are a helpful replacement for inorganic quantum dots, which are usually made up of toxic elements (Cd, Se, Pb, etc.).

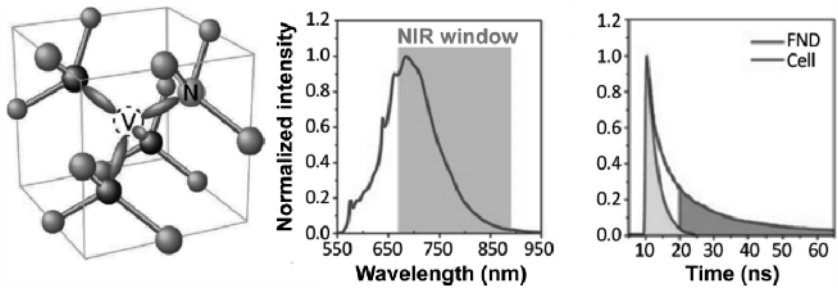

Figure 1.8. *Fluorescence of ND nanocrystallites containing NV defects*

COMMENT ON FIGURE 1.8.– *a) Structure of an NV defect resulting from the proximity of a nitrogen atom (impurity due to ND preparation) to a vacancy corresponding to the absence of a carbon atom. The lobes shown in purple correspond to the dangling bonds of the carbon atoms neighboring the vacancy V. b) Fluorescence spectrum of FND (size: 35 nm) obtained by laser irradiation at 532 nm. The pink rectangle represents the window for which the autofluorescence of biological tissue is negligible. c) Time difference between the fluorescence lifetimes of an FND (pink) and that of a biological cell due to the presence of endogenous fluorophores (green). The use of a 10 ns shift between excitation and detection neutralizes the effect of the underlying fluorescence of the biological medium. Adapted from [HSI 16].*

bombardment, vacancies (V) are produced; their migration and proximity to nitrogen atoms (N) leads to the formation of NV centers.

11 NV centers can exist in two forms: NV° and NV-. The preponderant NV- form is responsible for all magneto-optical properties due to its different spin numbers $m_s = 0$ and ± 1. NVs are characterized by a strong absorption band centered at 550 nm, and an intense fluorescence band around 685 nm, with high quantum yield (70%) [SCH 14].

1.2.2.2. *Boron-doped diamonds*

Nanodiamonds made up of a core of sp^3 carbons are insulators, with resistivity reaching values of the order of 10^{12} Ω cm^{-1}; the band gap, typically that of an insulating material, is equal to 5.47 eV [HE 19].

These characteristics are completely reversed when NDs are doped with boron. Unlike nitrogen doping, which does not exceed concentrations of 30 ppm, boron doping can be very high: it is possible to obtain concentrations of up to 30000 ppm, transforming the boron-doped nanodiamonds (BDD) into conductive materials suitable for use in electrochemistry. In cases of high boron doping (10^{20}–10^{21} atoms/cm^3), the resistivity of BDD is very low, corresponding to that of a semi-metal (10^{-3} Ω cm), meaning that this new material is suitable for use as electrodes. Lower levels of doping, around 10^8 atoms/cm^{-3}, give much higher resistivities of around 10^4 Ω cm [PAN 05].

BDDs containing very low levels of graphitic carbon constitute an exceptional material for electrodes [GAR 15a, HE 19], giving an electroactivity window, for both oxidation and reduction, which is much higher than that of platinum or glassy carbon. The reaction corresponding to the reduction of H^+ ions in an acidic medium with the release of dihydrogen occurs at –1.2 V compared to an SHE (standard H_2/H^+ reference electrode), and the reaction corresponding to the oxidation of water with the release of dioxygen occurs at 2.4 V/SHE, that is, in both cases, there is considerable overvoltage compared to thermodynamic equilibrium voltages[12]. This property, which is *a priori* counterproductive from a catalytic point of view, has been used for the oxidation of organic pollutants in water [PAN 05].

Several research groups currently consider that electrodes made of BDD films are the best available option for the destruction of organic materials [HE 19]. Their high resistance to corrosion, non-fouling of their surface due to their hydrophobic character and the very high overvoltage required for oxygen production mean that large quantities of $^{\bullet}OH$ radicals are produced and adsorbed on the electrode surface in the form of BDD-$OH^{\bullet}$. These highly reactive radical species have the effect of significantly increasing the oxidizing power of the electrodes with respect to organic compounds. Given their very high oxidizing power, their efficiency in wastewater treatment is much better than that obtained with platinum, graphite or even DSA

12 The reduction of H^+ ions on BDD in acid medium with the release of dihydrogen begins at −1.2 V/SHE (Standard Hydrogen Electrode) compared to −0.2 V on a glassy carbon electrode (GC); the reaction corresponding to the oxidation of water with the release of O_2 occurs at 2.4 V/SHE, instead of 1.5 V on GC. It should be noted that these properties, while they are helpful in terms of the oxidation of organic pollutants, represent a disadvantage in terms of energy for water splitting, which corresponds to the production of dioxygen and dihydrogen.

(a "dimensionally stable anode" by DeNora) electrodes, which are usually used for this kind of application [GAR 15b].

BDD electrodes can also be produced in the form of porous films, increasing the active surface of the electrodes and thus improving electrochemical performance. However, this raises a number of difficulties, principally in terms of the adhesion of the BDD film to the substrate (usually Ti or Si); this must be improved before the film can be used for long-term electrolysis operations [GAR 15b].

1.3. Carbon dots or carbon quantum dots

Carbon dots (CDs) or carbon quantum dots (CQD) are smaller than 10 nm in size, and consist of a core of graphitic-type sp^2 carbons, corresponding to fragments of graphene or graphene oxide (GO), linked together by sp^3 carbons. Their surface contains significant quantities of oxygen, essentially in the form of COOH, carbonyls and hydroxyl groups [LIM 15] (Figure 1.9). Discovered by chance during the preparation and purification of CNTs [XU 04], CDs rapidly attracted attention for their fluorescent properties, which mean they have the potential to be used as reagents for biomedical imaging. As in the case of NDs, their non-toxic nature presents an additional advantage, notably making them preferable to inorganic, heavy metal semiconductor-based quantum dots (QD) in many cases.

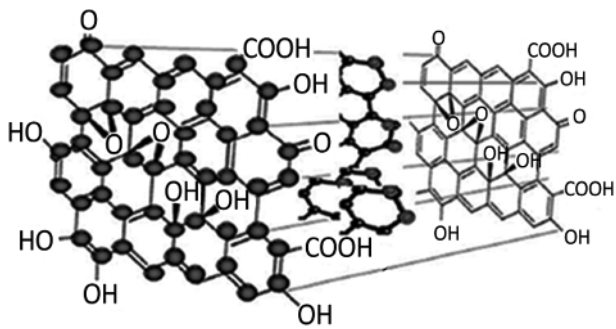

Figure 1.9. *Structure of carbon quantum dots (CQD) showing the association of graphene oxide and graphene fragments. Adapted from [DEM 13] and [LIM 15]*

1.3.1. *CQD production methods*

CQDs were first discovered in carbon soot. Produced by an electric arc discharge between graphite electrodes, CQDs were identified and isolated during electrophoresis separation of the various carbon NPs contained in the soot, thanks to

their fluorescence [XU 04]. Interest in these new fluorescent nanomaterials soon resulted in the development of other methods, such as laser ablation of carbon-based precursors [SUN 06, HU 09].

Many different production methods have been described in the literature [WAN 14b, FER 15, LIM 15]. As fluorescence is a key property of CQDs, the main objective is generally to obtain the best possible fluorescence properties at the lowest cost; different approaches result in different specific properties. The most common production methods involve pyrolysis, applied to hydroxylated or easily oxidizable chemical compounds (amino products), carried out by microwave irradiation of the precursor product to create carbonization. This is the simplest and least expensive method.

For instance, the carbonization of citric acid in the presence of amines, used as "passivation" agents[13], produces (after microwave irradiation) CQDs with very high monodispersity and a size distribution between 2.3 and 3 nm. Laser irradiation of a solution of these QDs at 360 nm produces an intense blue fluorescence, centered around 450 nm, with a high quantum yield (QY) of 30% [ZHA 12].

Another way of treating a hydroxylated organic precursor consists of successively using a highly concentrated acid (e.g., H_2SO_4) for its dehydrating power, followed by an acid with a strong oxidizing power (HNO_3), which breaks down bonds, leading to the formation of CQDs. Passivation of the CQDs using an amino compound is then used to increase the intensity of fluorescence of the CQDs [WAN 14b]. The same result can be achieved in a single step by heating polyethyleneimine (PEI), in contact with concentrated nitric acid, to 120°C with reflux [SHE 13a]. This technique has the advantage of being readily available and applicable to many organic precursors, but does not allow for very precise control of CQD sizes [WAN 14b].

A variant of alcohol degradation by electrochemical oxidation in a strongly basic medium has also been proposed, and this also results in fluorescent CQDs. This technique has the advantage of simplicity, insofar as CQDs can be obtained in a single step; it is possible to control CQD size using this approach, but unfortunately only a few compounds can be transformed using this method [LI 10a].

13 Citric acid is often chosen as an organic precursor because of the ease with which it can be dehydrated and degraded, a result of the presence of carboxyl and hydroxyl groups. The "passivation" amine probably acts as a nitrogen doping agent for the CQD core, and is thus responsible for an increase in the intensity of fluorescence; this effect is similar to that obtained by N-doping nanodiamonds.

The hydrothermal route has also been widely developed, and allows high-quality CQDs to be obtained at relatively low cost. This method consists of heat treating an organic precursor, placed in a sealed reactor, in the presence of high-temperature steam. The carbonization reaction can be carried out by choosing organic precursors such as glucose, citric acid or orange juice, along with a whole series of easily degradable natural compounds [WAN 14b].

When the organic precursor is pyrolyzed in a confined space, it becomes effectively possible to control the size of the CQDs. The use of nanoporous materials such as silica (in the form of microspheres) means that organic precursors can be inserted into the pores, which then act as nanoreactors. Hydrophilic CQDs are thus obtained by pyrolysis in air of silica microspheres (average diameter 1.3 μm, pore size 3.6 nm), soaked in salts and citric acid, at 300°C for 2 hours. After dissolving the silica using hydrofluoric acid, dialysis is used to recover CQDs, which are almost mono-disperse (sized between 1.5 and 2.5 nm). These are characterized by excellent photostability and high QYs in terms of fluorescence (23%) [ZON 11].

CQDs can be given a variety of different properties by doping or functionalizing the surface; one reason to do this is to increase the intensity of fluorescence. The ultimate goal is to match the QYs obtained using certain organic dyes or inorganic QDs such as CdSe, for which QY can reach 80% [LIM 15].

1.3.2. *Fluorescence properties of CQDs*

Unlike inorganic QDs, for which absorption is determined by the band gap, CQDs are characterized by a very broad absorption band resulting from plasmonic absorption of the π orbitals[14]. This absorption band covers a large part of the UV-visible spectrum and extends into the near infrared, thus intercepting a large part of the solar spectrum [FER 15].

Two main emission mechanisms, which are not always easy to identify, are responsible for CQD fluorescence. The first results from transitions between energy levels in domains composed of conjugated sp^2 carbons; the second, less evident, relates to surface defects present in CQDs. A third type of mechanism has also been identified, corresponding to an up-conversion of photons, where an emission is produced in the visible spectrum as a result of excitation in the red spectrum.

14 Plasmonic absorption corresponds to a collective excitation of delocalized π-electrons on multiple benzene rings.

It is widely accepted that photoexcitation of CQDs results in a separation of charges in the core carbons, and that their recombination with surface defects results in fluorescence. This also explains the high degree of variation in emissions, which is not strictly related to a confinement effect, specific to mineral semiconductor QDs (Figure 1.10).

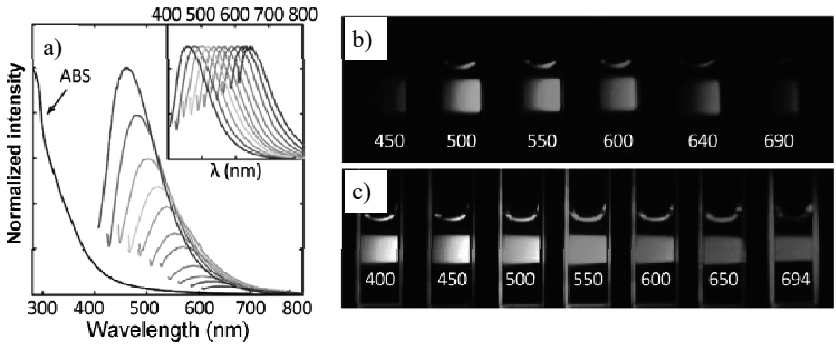

Figure 1.10. *Luminescence of an aqueous solution of CQDs produced by laser ablation of graphite powder*

COMMENT ON FIGURE 1.10.– *a) Absorption (ABS) and luminescence spectra obtained by excitation at different wavelengths (from 400 to 600 nm in 20 nm increments – from left to right) of poly(N-propionylethyleneimine-co-ethyleneimine) (PPEI-EI)-functionalized CQDs. Intensities are normalized with respect to quantum yields; the inset figure shows normalization with respect to peak intensity. b) Photographs of the luminescence of polyethylene glycol (PEG)-functionalized CQD solutions with a molar mass of 1500 and two amino groups – CH_2NH_2 (PEG_{1500N}) – at chain ends. Irradiation was applied at 400 nm, and the photographs are obtained after passing the emitted light through color filters of the indicated wavelengths (in nm). c) The same CQD solutions, photographed directly after irradiation at the indicated wavelengths (in nm). Adapted from [SUN 06].*

One of the most striking features of the fluorescence emission of CQDs is the way the emission spectrum depends on that of the source of excitation. Different explanations have been put forward for this dependence. The quantum size effect, defects and the surface states present in the CQDs, the presence of fluorophores with different degrees of conjugation and the radiative recombination of electron-holes due to clusters of sp^2 carbons enclosed in a matrix of sp^3 carbons all play a determining role, and may be responsible for fluorescence [WAN 10]. In general, the fluorescence QYs of most CQDs are in the range of 10%; however, in some cases, high yields of around 80% have been observed. These appear to be connected

to the presence of nitrogen, resulting from the precursors used during pyrolysis (citric acid and ethylene diamine) [ZHU 13].

Finally, for CQDs prepared under certain conditions, multiphoton absorption has also been observed. This corresponds to an upconversion of the emitted photons [LI 10b], which is an essential property for biomedical imaging; excitation can be produced in the near infrared spectrum (800–900 nm), offering very high levels of penetration of biological tissues (several mm). This property was discovered by the Sun group [CAO 07] for CQDs with sizes of the order of 5 nm, passivated by a nitrogenous polymer (polypropionylimine-co-ethylenimine) (Figure 1.11).

One or two-photon absorption can be obtained through excitation in the visible (458 nm) or near infrared spectrum (800 nm), respectively. The photoluminescence generated in the two cases is essentially the same, centered around 500 nm. The intensity of "two photon" luminescence is comparable to that of inorganic QD semiconductors, and verifies the law of linearity between the intensity of the emission and the square of the excitation power (Figure 1.11b).

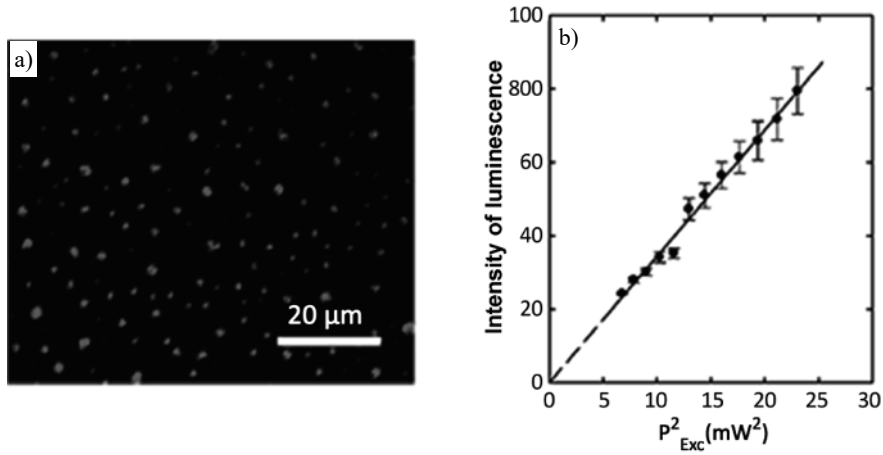

Figure 1.11. *Luminescence of CQDs deposited on a glass substrate*

COMMENT ON FIGURE 1.11.– *a) Image of CQDs excited by a femtosecond pulsed laser at 800 nm. b) Linear variation of the intensity of luminescence as a function of the square of the excitation power (P_{Exc}), characteristic of two-photon excitation. Adapted from [CAO 07].*

1.3.3. *CQD applications*

Given the ease with which CQDs can be produced and the numerous possibilities offered by surface functionalization, these have potential use in various multifunctional probes. For example, MRI and fluorescence imaging could be carried out simultaneously by combining magnetic and luminescent properties. This possibility has been illustrated by attaching nuclear resonance contrast agents (gadolinium complexes) to fluorescent CQDs [BOU 12].

Their solubility in aqueous media means that they are not only excellent diagnostic agents, but also very good vectors for transporting drugs to diseased biological cells; for instance, platinum-based anticancer drugs may be bound to CQDs [ZHE 14a].

Other applications have also been described [WAN 14b, HU 19] in domains as varied as analytical chemistry (sensor design), optoelectronics (photovoltaics and electroluminescence), and energy production and storage (supercapacitors and electrodes for lithium batteries).

1.4. Carbon nanotubes

Lijima [LIJ 91] was the first to demonstrate the formation of multi-walled carbon nanotubes (MWCNTs) by carrying out an electrical discharge between carbon electrodes in a reduced-pressure argon medium. Lijima thus obtained a mixture of MWCNTs with diameters ranging from 4 to 30 nm, around 1 μm long, and made up of two to seven concentric tubes. Single-walled carbon nanotubes (SWCNTs) were obtained shortly afterward, this time using cobalt-based catalysts [BET 93]. The structure of the walls of all of these nanotubes is identical to that of graphene: an assembly of a single layer of sp^2 hybrid carbon atoms in a regular hexagonal mesh.

Since CNTs were first produced and characterized, several teams have introduced different approaches to production and separation, described in the literature [GRO 07, HER 08, KOM 10, CHE 14c]. The main techniques used to produce CNTs include vaporizing carbon by laser ablation, electric discharge between graphite electrodes, catalytic chemical vapor deposition (CCVD), decomposition of CO under high pressure (HiPco process)[15] and the use of

15 The HiPco process was developed in the 1990s at Rice University. It allows high-purity SWCNT to be obtained by reacting carbon monoxide mixed with $Fe(CO)_5$ pentacarbonyl iron at high temperature (900–1,100°C) and under a pressure of around 30–50 atmospheres. The quantity of CNT produced using this process is of the order of 450 mg per hour, consisting of a mixture of SWCNT corresponding to about 10 distinct chiralities [BRO 01].

Co-doped silica nanoparticles (Co-MCM 41)[16]. The choice of catalyst and the technique used to fragment the carbon-based precursors play a determining role. The most widespread of these techniques is CCVD, which has the potential to produce large quantities of SWCNT and is thus best suited to production on a commercial scale (Figure 1.12).

Broadly speaking, the CVD technique consists of introducing a carbon source (ethylene, acetylene, toluene, CO, etc.) mixed with a carrier gas (H_2, argon) in vapor form into a reactor. The gas mixture, heated to a high temperature of at least 600°C, corresponding to the decomposition of the carbon-based precursor, comes into contact with the catalyst (in the form of metallic NPs) on which CNTs then develop.

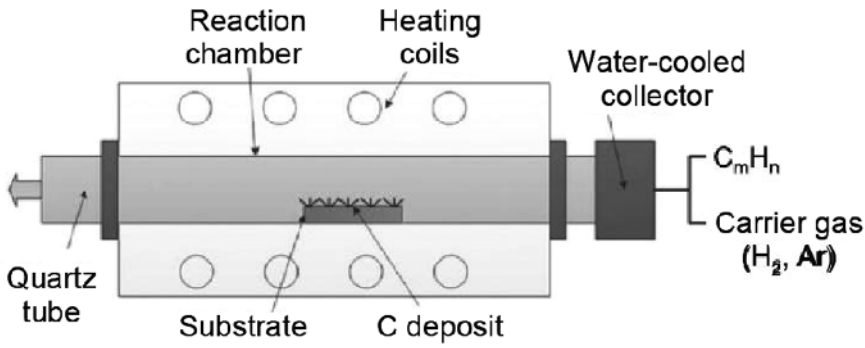

Figure 1.12. *Simplified diagram of the CVD apparatus used to produce CNTs. Adapted from Gore and Sane [GOR 11]*

The method is easily implemented on an industrial scale, as it only requires a tubular reactor, equipped with gas flow controllers, and an oven. However, the obtention of high CNT yields and well-defined chiralities remains problematic. The choice of a catalyst with a particular crystal geometry is crucial; a considerable number of different transition metal catalysts have been tested and described in the literature [WEN 10, TES 11, CHE 14c, WAN 15a, JAN 16].

The electrochemical route is also being investigated as a potential means of producing large quantities of carbon nanomaterials, such as graphene, carbon fibers, CDs and CNTs. One recent solution involves reducing CO_2 in the form of molten carbonate; this approach, developed by the Pint group for CNT production, has the

16 MCM-41 is a specific zeolite with pores that can be "tuned" between 2 and 10 nm. After depositing a thin layer of cobalt on the inner walls of the zeolite, it can be used as a nanoreactor for the production of SWCNT [LIM 03].

merit of converting CO_2 into valuable products [DOU 17]. Unlike in previous work, the authors showed that better selectivity with regard to CNT size could be achieved by using a thin layer of iron, deposited on a stainless steel cathode, as a catalyst. In contact with the molten electrolyte (Li_2CO_3), that is, at temperatures above 720°C, the thin metallic layer generates iron NPs on which CNTs will grow. The iron NPs grow as a function of electrolysis time and thus the diameter of the CNTs also increases; this makes it possible to control CNT size by adjusting electrolysis time. With an initial iron layer of 0.5 nm thickness, the average diameter of CNTs produced is 12.5 nm after 3 minutes and 23 nm after 1 hour of electrolysis using a current of around 100 mA/cm^2 [DOU 18] (Figure 1.13).

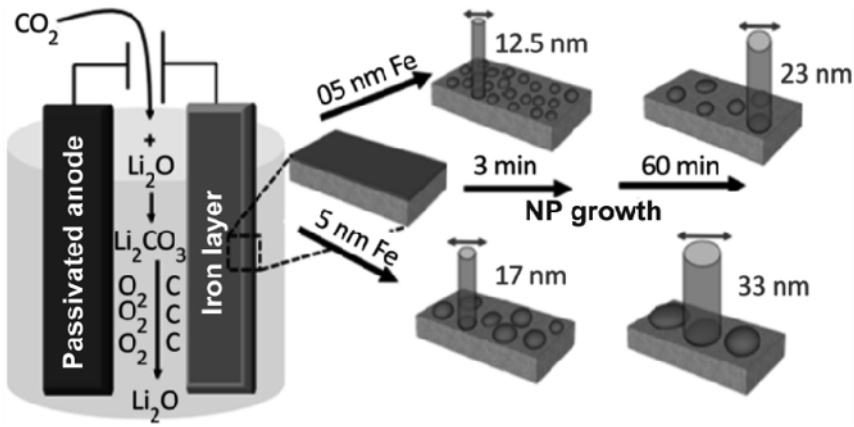

Figure 1.13. *Schematic illustration of the electrolysis setup for CNT production*

COMMENT ON FIGURE 1.13.– *a) The cathode is covered with a thin layer of iron on which carbon is deposited. The anode is passivated by a layer of alumina on which O_2 is released. b) On contact with the electrolyte (Li_2CO_3), the iron layer generates iron NPs; the size of these NPs increases as a function of electrolysis time, as does the size of the CNTs. The diameter of the CNTs is calibrated by that of the iron NPs. Adapted from [DOU 18].*

According to the authors, the cost of producing CNT in this way is much lower than when using CVD techniques, and the yields are also higher. However, the process still needs to be refined in order to obtain CNTs of smaller diameter, and to increase selectivity.

Most of the techniques used result in CNT mixtures containing both MCVNTs and SWCNTs, with different architectures corresponding to different chiralities. Research into improving separation methods is still ongoing; researchers also aim to develop new catalysts which offer better selectivity in producing CNTs with a given configuration or chirality. Various theoretical models have been developed to further understanding of CNT formation mechanisms at an atomic level, notably in terms of the auto-assembly phenomena by which carbon atoms form CNTs and by which these CNTs grow [PAG 15].

1.4.1. *Chirality of carbon nanotubes*

The formation of an SWCNT may be seen as the result of "rolling up" a graphene fragment along a given path, defined by a C_h vector (Figure 1.14).

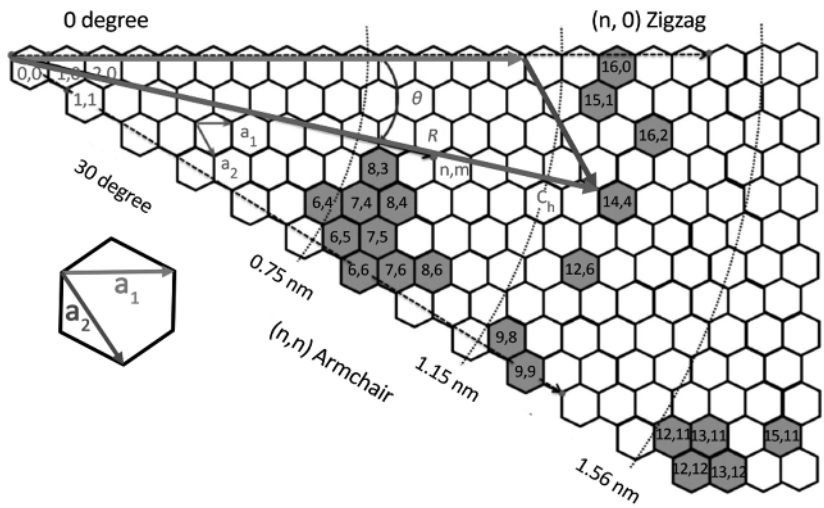

Figure 1.14. *Diagram showing the formation of an SWCNT defined by rolling up a graphene fragment along the chiral vector $C_h = na_1 + ma_2$*

COMMENT ON FIGURE 1.14.– *In the case shown in the figure, the C_h vector (red arrow) is equal to $14a_1 + 4a_2$ and corresponds to the formation of an SWCNT of chirality (14,4). The C_h vector is at an angle Θ with respect to the a_1 vector axis and defines an R (rectus)-type chirality. The diameter of the SWCNT (4,14) is the same as that of the SWCNT (14,4) with S (sinister) chirality. The hexagons shown in blue correspond to the most common chiralities of synthetically obtained CNTs with diameters between 0.7 and 2 nm. Adapted from [WAN 15a].*

The vector C_h, known as the chirality vector, is defined by the vector sum of two vectors $\mathbf{a_1}$ and $\mathbf{a_2}$ which characterize the network, such that C_h is equal to n $\mathbf{a_1}$ + m $\mathbf{a_2}$, where the angle between $\mathbf{a_1}$ and $\mathbf{a_2}$ is 60°. A CNT of chirality (n,m) is thus obtained by rolling up the graphene fragment along the direction of the vector C_h in such a way that it connects the two ends of the vector C_h. It follows, from this construction, that the circumference of the SWCNT is equal to the length of the vector C_h [BAC 02].

Chirality is particularly important because it has a decisive effect on the conductive properties of CNTs and, consequently, determines their use in fields such as nanoelectronics, photovoltaics and energy storage.

Within each family of SWCNTs with distinct chiralities (n,m), there are two limit forms: "armchair" (n,n) or "zigzag" (n,0); these correspond to winding directions at an angle Θ of 0° or 30°, respectively (Figure 1.15). Note that the armchair configuration offers metal-like conductivity. The "zigzag" (n,0) configurations, like SWCNTs of chirality (n,m), also possess metal-like conductivity when the difference between n and m is a multiple of 3 [MAU 05], and are semiconductors when this is not the case. The band gap widths are less than 1 eV and decrease as the diameter of the CNT increases [ODO 98].

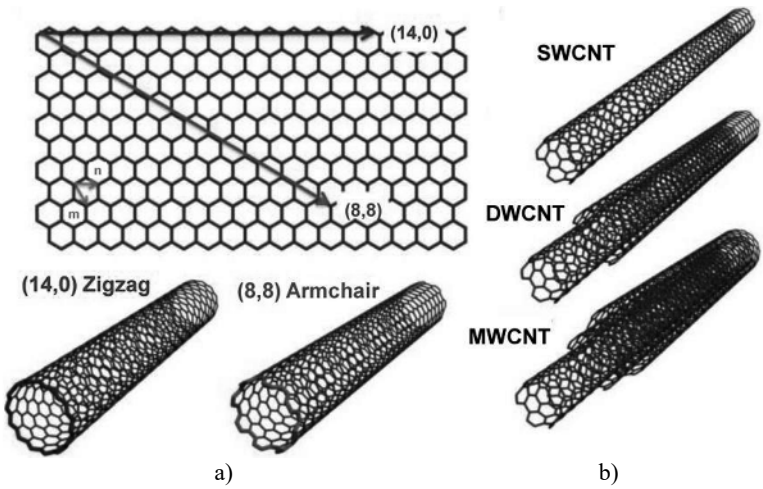

Figure 1.15. *Examples of different CNT configurations. a) Examples of two SWCNTs, (14,0) and (8,8), constructed from a single sheet of graphene and coiled along the vectors (14,0) (red) and (8,8) (green), corresponding to the zigzag and armchair forms. b) Images of single-, double- and multi-walled CNTs (SWCNT, DWCNT and MWCNT). Adapted from [SCH 11]*

Each of these configurations (n,m) has a distinct corresponding Raman spectrum and distinct CNT diameter, making it possible to identify them. The frequency of the Raman RBM (Radial Breathing Mode) band, corresponding to the radial mode of vibration of the nanotube (ω_{RBM}), is related to the diameter (d) by the relation $\omega_{RBM} = A/d + B$, where A and B are two experimentally determined constants [BAC 02, MAU 05].

Given the importance of chirality in terms of conductive properties, significant efforts have been made to develop separation methods [LIU 10a] along with preparation techniques for producing SWCNTs of defined chirality in the most selective way possible.

1.4.2. *Mechanistic models of CNT growth*

The growth of CNTs with a certain chirality is known to be closely correlated to the crystal structure of the catalyst and to the arrangement of atoms in the different planes of the crystal [TES 11]. The first models of CNT growth, VLS (Vapor Liquid Solid) followed by VSS (Vapor Solid), draw on the mechanisms at play in carbon fiber formation. According to these models, the carbon-based gaseous precursor, heated to a temperature of around 600°C, dissociates on contact with the catalyst, producing C atoms; these diffuse onto the surface of the catalyst and will then recombine, triggering the growth of a carbon nanofiber or CNT.

Numerous observations using high-resolution transmission electron microscopy (HRTEM), XPS (X-ray photo-electron spectroscopy) or EELS (electron energy loss spectroscopy) analysis, taken alongside theoretical calculations and molecular dynamic modeling, confirm that this general scheme is applicable to CNT growth (Figure 1.16).

However, CNT chirality still depends on a range of parameters such as the size of the NPs which make up the catalyst, the atomic composition of the alloy, the temperature at which the reaction occurs and the nature of the gas precursor.

For example, SWCNTs with a zigzag configuration (16.0) and a diameter of 1.25 nm are difficult to obtain in large quantities, but production techniques have been considerably improved in recent years by using W_6Co_7 crystals with specific cutting planes (116) [YAN 15]. According to the authors, this arrangement of the catalyst atoms results in a kind of “template” effect that directs the recombination of the carbon atoms toward the preferred CNT form (16,0), giving yields of around 80%.

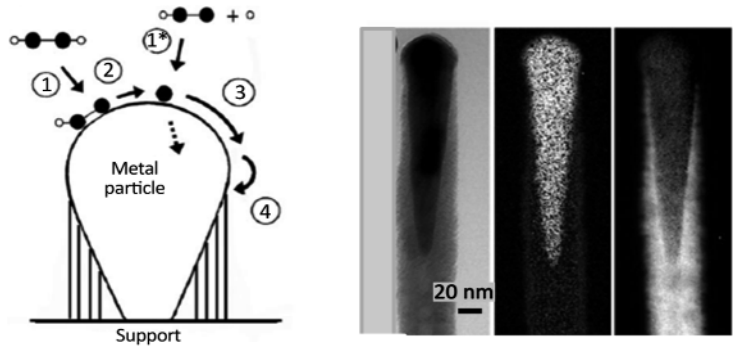

Figure 1.16. *Different steps in CNT growth using the VSS mechanism*

COMMENT ON FIGURE 1.16.– *a) (1) Adsorption; (2) decomposition of the carbon-based precursor, (3 and 4) diffusion of carbon atoms at the surface of the catalyst; (1*) partial dehydrogenation of the precursor. b) Bright field TEM. c) EELS image of Ni (absorption at 854 eV corresponding to the edge of the L band). d) EELS image of C (absorption at 284 eV corresponding to the edge of the K band). Adapted from [HOF 05].*

More recently, Wang *et al.* [WAN 18] have shown that high levels of selectivity can also be obtained by using nickel, cobalt or iron sulfates as catalysts; this amounts to introducing sulfur indirectly into the catalysts (Figure 1.17).

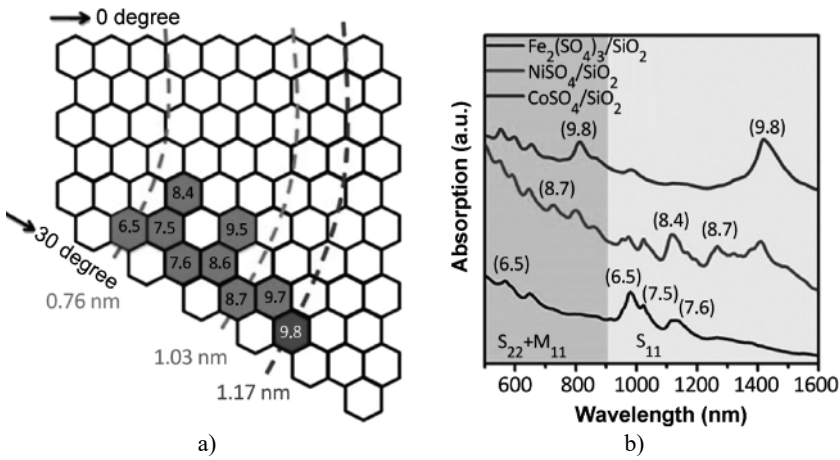

Figure 1.17. *Characterization of SWCNTs synthesized using different catalysts (mixtures of metal sulfates and SiO_2)*

COMMENT ON FIGURE 1.17.– *a) Distribution of the different SWCNTs (n,m) synthesized using ferric sulfate (green), cobalt sulfate (blue) and nickel sulfate (red) on a chiral "map". b) Near IR and IR absorption of different SWCNT mixtures obtained following separation by complexation using sodium dodecyl benzene sulfonate (SDBS) followed by ultracentrifugation. Adapted from [WAN 18].*

Thus, a dispersion of silica NPs impregnated with ferric sulfate ($Fe_2(SO_4)_3/SiO_2$) results, after heating, in a mixture of iron oxides and silicates, producing SWCNTs of chirality (6,5) and diameter 0.76 nm. Similarly, the replacement of ferric sulfate by nickel or cobalt sulfate results in high yields of larger diameter CNTs with chiralities (8,7) and (9,8), respectively.

These results confirm previous observations that the presence of a small amount of sulfur is necessary to stabilize the size of the metal catalyst particles, which are themselves critical for the growth of CNTs in SWCNTs or MWCNT form [JAN 16].

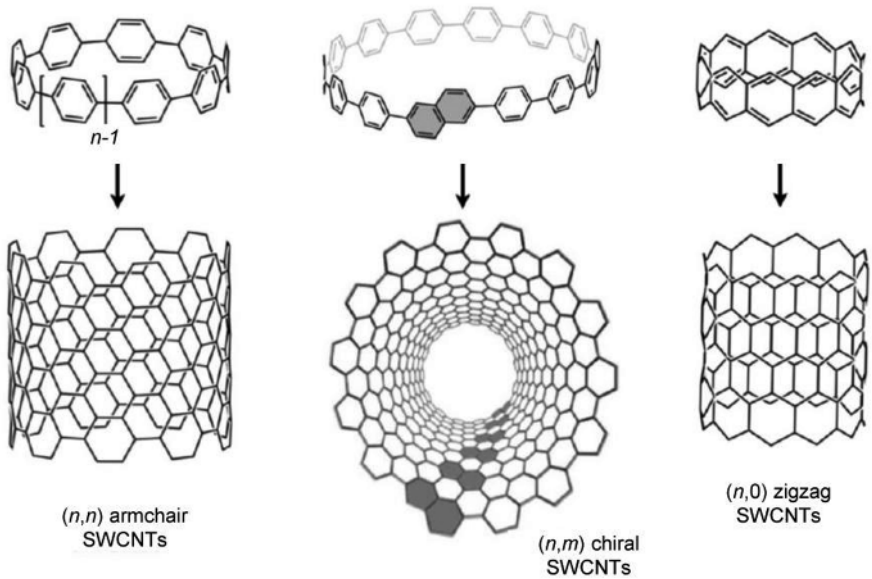

Figure 1.18. *Illustration of CNT growth from cycloparaphenylene (CPP). a) Armchair SWCNT (n,n) obtained from a CPP. b) SWCNT of chirality (n,m) obtained from a CPP into which a naphthalene group has been inserted. c) Zigzag SWCNT (n,0) which may be produced from n-acenes. Adapted from [PAG 15]*

This catalyst "template" effect has also been demonstrated using organic derivatives, such as cycloparaphenylene (CPP) carbon rings, which constitute the

shortest segment of a CNT with an "armchair" configuration, in the place of metal crystals. In this case, the reaction is carried out at a temperature of 500°C, using ethanol as the carbon source. The growth of the CNT is thus calibrated to that of the carbon nanoring, meaning that the diameter of the CNTs can be adjusted by acting on the size of the CPP (Figure 1.18a) [OMA 13].

Note, however, that the level of selectivity obtained using this technique is not as high as those seen previously. For example, using a CPP made up of 12 phenylene nuclei ([12]-CPP) with a diameter of 1.7 nm results in a mixture of CNTs with diameters which mostly fall within a range of 1.7–1.3 nm; the most common diameter is 1.7 nm (over 20%).

A naphthalene group can be introduced into the ring [OMA 11] to break the symmetry and obtain chiral SWCNTs (Figure 1.18b). The use of a cyclic n-acene as a precursor is expected to result in SWCNTs with a zigzag configuration (Figure 1.18c), but at the time of writing, this hypothesis has yet to be tested.

1.4.2.1. *Classic separation methods for SWCNT mixtures*

Affinity or steric exclusion chromatography[17], electrophoresis and ultra-centrifugation are among the most common techniques used to separate materials of different shapes and sizes.

In the case of CNT, centrifugation techniques are most widespread due to their high efficiency, low cost of implementation and scalability.

The most popular method combines ultracentrifugation with an aqueous density gradient medium (DGU) which is widely used in biology. This technique has proven to be particularly effective for separating and sorting SWCNTs with determined chiralities.

This approach draws on small differences in the buoyancy density of particles dispersed in an aqueous solution with a density gradient. This density gradient is obtained by mixing a high-density compound with water in such a way that the density of the solution increases from the surface to the bottom of the solution. Under centripetal force, the analyzed species migrate toward the position at which the density of the species is equal to that of the solution, which has the effect of distributing the components of the mixture across different zones of the solution.

17 Steric exclusion chromatography is based on the difference in size of particles or macromolecules, whereas affinity chromatography is based on differences in physicochemical interactions between molecules and the chromatographic support.

As CNTs are hydrophobic, a surface modification is necessary to make them hydrophilic and facilitate their dispersion in an aqueous media. One approach involves the adsorption of polyaromatic derivatives, particular oligonucleotide sequences; a more common method involves the adsorption of amphiphilic surfactants such as sodium dodecyl sulfate (SDS) or sodium cholate (SC). These surfactants may coil and adsorb onto the CNT, transforming the CNT-surfactant mixture into a hydrophilic species compatible with the aqueous immersion medium. CNTs with very high purity levels can then be obtained following ultracentrifugation and washing (Figure 1.19).

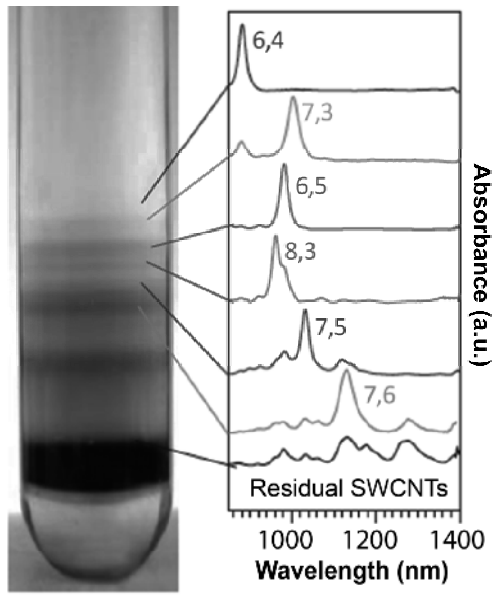

Figure 1.19. *Separation of SWCNTs of structure (n,m) using ultracentrifugation, applied to a mixture of SWCNTs obtained using the HiPCo method*

COMMENT ON FIGURE 1.19.– *a) The centrifuge tube initially contains seven distinct layers of water-iodixanol solutions with a concentration increasing from 15% to 30% by weight from the top to the bottom of the tube. After 18 h of centrifugation at 268000 g, different sedimentation regions are obtained, each containing SWCNT of defined chirality. b) Raman spectroscopy analysis of each colored slice confirms the presence of SWCNT which mostly correspond to well-defined (n,m) chiralities: (6,4), (7,3), (6,5), (8,3), (7,5) and (7,6). Adapted from [GHO 10].*

Various authors have obtained good results separating SWCNTs using this method [ARN 06, GHO 10, GRE 11]. Ghosh *et al.* [GHO 10] separated and isolated SWCNT from a mixture of CNT obtained using the HiPco method. Separation is carried out in a centrifuge tube in which several layers of liquid with distinct density gradients have been added, corresponding to solutions of increasing concentrations of iodixanol[18] in water, ranging from 15% (w/v) at the top of the tube to 30% (w/v) at the bottom of the tube.

1.4.3. *CNT arrays aligned horizontally or perpendicularly to a planar substrate*

CNTs which are horizontally or perpendicularly aligned with respect to a planar substrate present different properties and are thus suited to different applications. The excellent conductivity of vertically aligned CNTs, along with their ability to withstand very high electric currents, means that they can be used as vertical connectors between different layers of electronic components in 3D integrated circuits, using the TSV (Through silicon via interconnect) concept[19] [WAN 11]. This form is also ideal for use in designing cathodes which emit electrons under the effect of an electric field. Conversely, horizontal alignments are better for use in field effect transistors (FETs), which can be used in designing sensors, for example, for detecting traces of various chemical compounds. Substantial progress in this area has made it possible to obtain defect-free alignments, thanks to a particular set of experimental conditions, resulting in physical, mechanical and electronic properties which are close to the theoretical values [ZHA 17c].

1.4.3.1. *Vertically aligned CNT arrays*

Chhowalla *et al.* [CHH 01] were among the first to create vertically aligned CNT (VACNT) arrays on a silicon substrate using the Plasma Enhanced Chemical Vapor Deposition (PECVD) technique. They showed that the thickness of the catalyst layer, the deposition temperature and the proportions and flow rate of the acetylene/ammonia gas mixture play a decisive role in the vertical growth of the CNTs and in determining their structure [CHH 01]. Numerous variants have been tested, acting on the nature of the gaseous precursor and the catalyst, while maintaining the CVD technique; this has resulted in the development of VACNTs with various surface densities and lengths of up to several mm [HAT 04].

---

18 Iodixanol is a neutral iodine compound with formula $C_{35}H_{44}I_6N_6O_{15}$ which is used to create density gradients. It is available commercially in the form of an aqueous solution of 60% concentration (w/v), corresponding to a density of 1.32 g/ml.

19 The term VIA, used in nanoelectronics, stands for vertical interconnect access.

Zhang *et al.* [ZHA 08] suggested a particularly interesting use of VACNTS for producing electrochemical supercapacitors, formed by inserting redox NPs of manganese oxide (MnO_2) in contact with VACNTs deposited on a tantalum collector electrode (Figure 1.20). In this case, the VACNTs guarantee strong electrical contact between the metal electrode and the redox species inserted between the CNTs; furthermore, this results in a hierarchical porosity of the whole (macropores between the CNTs and micropores in the Mn oxides), which promotes the electrochemical diffusion of ions.

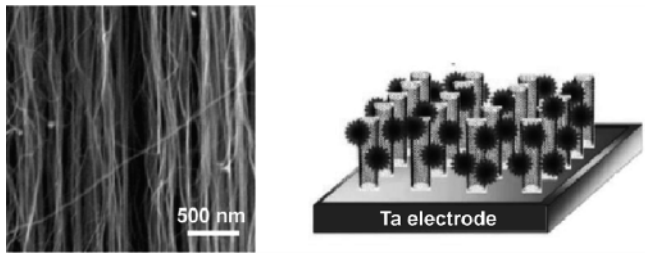

a) b)

Figure 1.20. *Diagram of a "composite" electrode, made up of a "forest" of SWCNTs (approximately 35 µm long) into which NP of MnO_2 have been inserted*

COMMENT ON FIGURE 1.20.– *a) SEM image of the VACNT array obtained by CVD (catalyst: iron phthalocyanine, carbon precursor: ethylene, CNT formation temperature: 550°C). b) Insertion scheme of MnO_2 NPs (electrodeposited from $MnSO_4$ solutions) inside the VACNT array. Adapted from [ZHA 08].*

Comparison with other composite electrodes, for example, with activated carbons (AC), clearly shows that the kinetic behavior of the VACNT solution is superior. While the specific capacities of the MnO_2/VACNT composite electrode and that of a MnO_2/AC electrode are comparable at low current densities (about 200 F/g each), the difference at high discharge intensities is considerable. Thus, for current densities of 10 A/g, the MnO_2/VACNT electrode maintains a capacity of around 130 F/g, whereas that of the MnO_2/CA electrode drops rapidly to around 50 F/g. For even higher intensities of 70 A/g, the capacity of the MnO_2/VACNT electrode is 101 F/g, making it particularly suitable for high-power applications [ZHA 08].

1.4.3.2. *Horizontally aligned CNT arrays*

Obtaining aligned CNT arrays on a substrate is essential for the production of various electronic components. Liu and coworkers were among the first to show that the orientation of CNTs could be controlled by CVD, by rapidly increasing the

temperature of the gas stream, consisting of a CO/H_2 mixture, to 900°C [HUA 03]. In this way, it is possible to obtain 2D arrays of aligned SWCNTs, several mm in length, from monodisperse Fe/Mo NPs deposited on the surface of a Si/SiO_2 substrate.

Improvements to the process have since been made by Li and coworkers, resulting in the production of ultralong, horizontally aligned SWCNTs; these are highly useful for producing ultra-resistant fibers [JIN 07] (Figure 1.21).

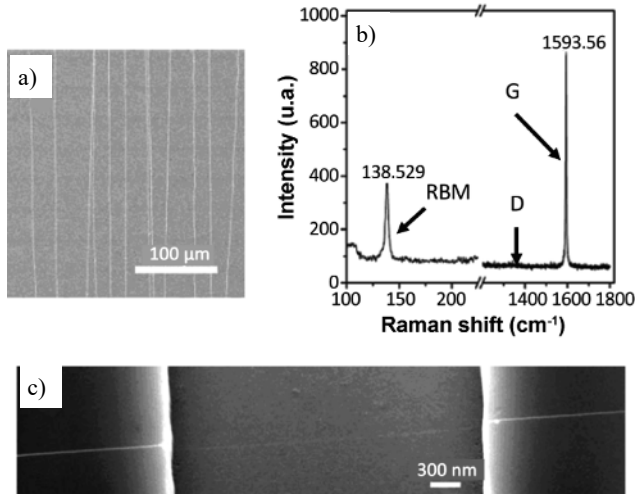

Figure 1.21. *Horizontally aligned SWCNT array on silicon substrate*

COMMENT ON FIGURE 1.21.– *a) SEM image showing the alignment and spacing of SWCNTs. b) Raman spectrum of a specific SWCNT. The RBM vibration corresponds to an SWCNT with a diameter 1.8 nm. The very low intensity of the D-band at 1350 cm^{-1} is an indication of the absence of defects in the CNT. c) SEM image of an SWCNT crossing a microtrench. Adapted from [JIN 07].*

They have shown that has shown that by slowly circulating the gaseous carbonaceous precursor ($CH_4 + H_2$) above the catalyst (iron and molybdenum NPs) at a very high temperature (970°C), CNTs grow steadily and can reach several cm in length [JIN 07].

One particularity of this growth mode is the floating character of the CNTs, which have the capacity to cross micro-trenches (~3 µm wide and 0.5 µm deep) or micro-obstacles without interrupting their progression; this is due to the fact that a catalyst NP remains attached to the end of the growing tube. Raman spectra confirm

that the SWCNT obtained in this way present very few defects. High-quality horizontally aligned CNT (HACNT) arrays have also been obtained using iron-based catalysts. One advantage to this approach is that nanotubes can self-repair during formation; this eliminates most of the defects which may result in a loss of useful properties. The carbon source is a weakly humidified mixture of methane and hydrogen; the substrate is a silicon plate, and the gas mixture is maintained at a temperature of between 900°C and 1000°C [ZHA 17c].

1.4.4. *Key properties and applications of CNTs*

Space does not permit us to provide a full list of properties, current and future applications of CNTs here; an excellent summary has been published by De Volder *et al.* [DEV 13]. The diversification of preparation methods, notably the development of HACNT or VACNT assemblies and the production of CNTs of several cm length, has considerably increased the field of applications. Self-supporting films of agglomerated CNT with a paper-like form (buckypaper), with excellent properties from both a mechanical and electrical standpoint, are now available commercially and have a wide range of potential applications. Sheets of buckypaper (6 μm thick) can be manufactured by simple vacuum filtration of an MWCNT suspension; the film obtained has an elasticity modulus of 3 GPa and a conductivity of 2.10^4 S/cm depending on the state of deformation, meaning that it could be used in motion detection sensors [DEG 17].

CNTs have a wide range of uses in fields such as nanoelectronics, energy and biomedicine, where their exceptional electrical, mechanical and thermal properties are particularly helpful. These properties have contributed to the success of CNTs, to the point where many companies have developed large-scale production techniques. Over the space of a few years (2004–2011), world CNT production increased from 200 kg to 4500 tons per year, a 22500-fold increase [DEV 13]. However, it should be noted that a number of companies have recently stopped producing CNTs, presumably due to high production costs. The average cost of SWCNTs remains very high; prices depend on packaging methods and vary between manufacturers. In 2020, the cheapest SWCNTs fetched between $80 and $100/kg, while industrial grade MWCNTs cost between $200 and $400/kg.

1.4.4.1. *Electrical properties*

CNTs are characterized by high conduction due to their metallic nature. Wei *et al.* [WEI 01] have shown that MWCNTs can withstand current densities of more than 10^9 A/cm^2 over periods of two weeks, at temperatures of around 200–250°C, with no degradation of the CNT or variation in conductivity. These conductance properties are a result of ballistic-type conduction mechanisms, different from the classical electron displacement mechanisms found in metals. Semiconducting CNTs

are also characterized by exceptionally high electron and hole mobility, far beyond that observed in silicon, reaching up to 79000 $cm^2\ V^{-1}\ s^{-1}$ [DÜR 04]. Bandwidth gaps are inversely proportional to the diameter of the CNT and are of the order of 1 eV for diameters of 1 nm, comparable to those of silicon [KAT 99].

1.4.4.2. *Thermal conduction*

CNTs are also excellent thermal conductors, but only along the axis. For a SWCNT 2.6 µm in length and 1.7 nm in diameter, thermal conductivity of 3500 $Wm^{-1}\ K^{-1}$ has been measured; that of copper, considered to be a very good thermal conductor, is only around 385 $Wm^{-1}\ K^{-1}$ [POP 06]. On the other hand, the thermal conductivity of CNTs in a radial direction is very low, only 1.52 $Wm^{-1}\ K^{-1}$, meaning that they can almost be considered thermal insulators in this direction [SIN 05]. This difference in thermal properties between the two orientations is the reason why CNT films, where assemblies are arranged randomly on a surface, have a thermal conductivity of the order of 1500 $Wm^{-1}\ K^{-1}$ [KOZ 17]. Note that these CNTs can withstand temperatures of up to 2800°C in a vacuum and up to 750°C in air.

1.4.4.3. *Mechanical properties*

Theoretical calculations performed on ideal CNT structures display exceptional mechanical characteristics, with a tensile strength of 100 GPa (10^{11} Pascal), a Young's modulus of 1 TPa (10^{12} Pascal) and a breaking strain of 18%. These values were obtained for defect-free CNTs of several cm in length. In terms of mass per kilogram, systems of this type have the potential to store a mechanical energy density equivalent to 1125 Wh/kg, and an immense (theoretical) power density of 144 MW/kg, far beyond that of all known devices – such as electrolytic capacitors and lithium batteries – in terms of performance. The power densities of these systems do not exceed 10 kW/kg and 1 kW/kg, respectively, and their respective energy densities of 3–4 Wh/kg and 100–200 Wh/kg are also much lower than the values obtained for CNT [ZHA 11].

Much work has also been carried out concerning the use of CNT as reinforcing fibers for polymers, resulting in the production of CNT/polymer composites. The techniques used to manufacture these composites, as well as their electrical and mechanical properties, have been described in detail in the literature [COL 06, SPI 10, SUN 13, CHE 17]. These properties not only depend on the nature of the polymer, the synthesis method and the dimensions of the CNTs, but also on the alignment of these CNTs and the degree of dispersion of the CNTs in the polymer matrix.

In practice, CNT/polymer composites are obtained by introducing CNTs into either a polymer solution or the polymer itself in a molten state. If the polymer is insoluble and infusible, the composite material can be synthesized by adding the

corresponding monomer to the CNT suspension, then carrying out polymerization *in situ*. One further way of synthesizing a composite is to inject a polymer solution into a CNT array.

1.4.4.4. *Black body properties of CNTs*

Near-perfect black body properties have been observed using a vertical assembly of CNTs on a silicon substrate, created using the CVD process and with humidified ethylene as the carbonaceous derivative precursor [MIZ 09] (Figure 1.22).

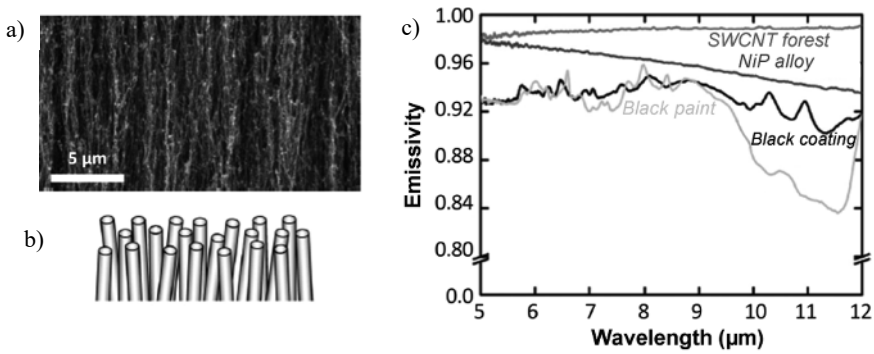

Figure 1.22. *SWCNT "forest" deposited vertically on a silicon substrate*

COMMENT ON FIGURE 1.22.– *a) Profile image of the CNT deposit. b) The slight defect in parallelism between SWCNTs is probably responsible for the very high emissivity. c) Emissivity of the SWCNT forest compared to that of NiP alloy, black paint and black coating. Note that beyond 9–10 µm, the emissivity of NiP, carbon black and black paint decreases significantly in comparison with SWCNTs. Adapted from [MIZ 09].*

Emissivity of 98%–99% is obtained across a whole spectral band from UV (200 nm) to far IR (200 µm)[20], much higher than values obtained for graphite or carbon black (between 80% and 85%); this level of performance is also very rarely obtained using other products, such as black paints or arrays of nickel-phosphorus alloy needles, which are particularly reputed for their capacity to absorb light radiation.

20 The emissivity of an object under irradiation is defined as the ratio between its emitted energy and that of the ideal black body.

1.4.5. *Conclusion*

The strategic importance of CNTs, as a family of nanomaterials, has become increasingly apparent since their first discovery by Lijima in Japan in 1991. Their exceptional electrical and mechanical properties have given rise to a significant number of applications, a development promoted by widespread commercialization. However, obtaining large quantities of CNTs with high purity levels and specific chiralities still presents a challenge. Current research is directed at identifying new catalysts to improve production on an industrial scale and to further broaden the field of applications, all while lowering production costs.

1.5. Graphene

Graphene was long considered as an ideal model, used in theoretical studies of 2D materials. A graphene fragment was first isolated by Geim and Novoselov [GEI 07] by mechanical exfoliation of a graphite sheet[21] (Figure 1.23).

Remarkably, the graphene film obtained in this way (with dimensions of around 10 μ) turned out to be extremely stable – contrary to previous predictions – and easy to subject to a whole series of electrical and mechanical measurements. Moreover, a monolayer of graphene can be easily identified using Raman spectroscopy; a characteristic line (G) appears at 1584 cm^{-1}, with a further line (2D or D′) at around 2700 cm^{-1}, the width of which increases as the number of graphene layers increases [FER 06, GRA 07].

Graphene presents exceptional physical, chemical and mechanical properties, leading many to consider it as the material of the 21st century. Its unprecedented electrical properties make it a material of choice for electronics, and have considerably improved the performance of various devices used in electronics and optoelectronics, in the energy sector and for biomedical analysis. The first graphene-based transistors were built in the 2010s. However, as Schwierz indicated [SCH 10], the fact that the band gap of graphene is zero means that it cannot be used as a FET for digital logic operations. A band gap opening is necessary for these applications; nevertheless, one solution is to use very fine graphene ribbons, for which band gaps of 200–300 meV have been observed. Graphene has been used in developing new

21 Although this technique may appear simple, the graphene sheet deposited on a Si substrate covered with a thin layer of SiO_2 only becomes visible if there is an optical contrast between the silica and the graphene. This only occurs if that the thickness of the silica layer is perfectly matched to that of the graphene sheet. Geim and Novoselov (who were awarded Nobel Prize for Physics in 2010) acknowledged that they were only able to identify the presence of a graphene monolayer through a fortunate combination of circumstances [GEI 07].

photonic and photoelectronic devices [BON 10], and has also been put forward as a potential component for batteries and capacitors (see Chapter 3) or photovoltaic cells (see Chapter 4) [BRO 11]. It also has promising applications in biosensors [PUM 11].

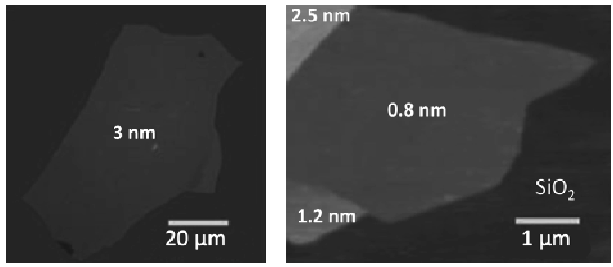

a) b)

Figure 1.23. *Graphene films deposited on a Si substrate covered with a thin layer of SiO_2*

COMMENT ON FIGURE 1.23.– *a) Photograph (in white light) of a multilayered graphene fragment, thickness 3 nm. b) AFM image of different thicknesses of graphene fragments. The central section, with a thickness of 0.8 nm, corresponds to a double layer of graphene. A thickness of 0.4 nm, corresponding to a single layer, is detected at the very bottom of the film. Adapted from [NOV 04].*

1.5.1. *Electrical properties of exfoliated graphene*

Graphene, which consists of an assembly of sp^2 carbons arranged in a perfect 2D hexagonal lattice, may be assimilated to a semiconductor material which has an energy band gap of zero (Figure 1.24).

The conductivity of graphene and the mobility of electrical charges are both extremely high, and these essential properties are what set graphene apart from other 2D materials, such as $NbSe_2$ or MoS_2. It can be doped with either positive or negative charges, by simply applying an electrical field. In contrast, the application of an electrical field in other 2D semiconductors only modulates the concentration of electrons, without reversing the passage from negative to positive charge carriers according to the polarity of the electrical field [NOV 05a]. The charge carriers in graphene do not obey the laws of non-relativistic classical quantum mechanics deduced from the Shrödinger equation; instead, they obey the laws of relativistic Dirac physics, in which low-energy electrons are assimilated to massless quasi-particles, with spin of 1/2, corresponding to 2D Dirac fermions. Their electrical properties have been extensively described in numerous articles by Geim

and Novoselov [GEI 07] and Novoselov *et al.* [NOV 05b]. It is possible to interpret all of the observations relative to the electrical properties of graphene – notably those concerning the Hall effect – using this theory.

Dirac physics involves conical valence and conduction bands, known as Dirac cones. These intersect in the space of wave vectors k associated with these particles at a singular point of zero energy and zero charge (the Dirac point). One of the paradoxes inherent in this theory is the existence of non-zero conductivity at the Dirac point despite the fact that the corresponding charge density is zero (Figure 1.24a).

The differences in conductivity between graphene and 2D semiconductor materials such as $NbSe_2$ and MoS_2, each incorporated as a channel in a FET, are clearly shown in Figure 1.24b. In the case of graphene, the conductivity variation curve is perfectly symmetrical with respect to the gate voltage $V_g = 0$ V, while for bulk $NbSe_2$ and MoS_2, we observe a monotonic variation in conductivity as a function of V_g.

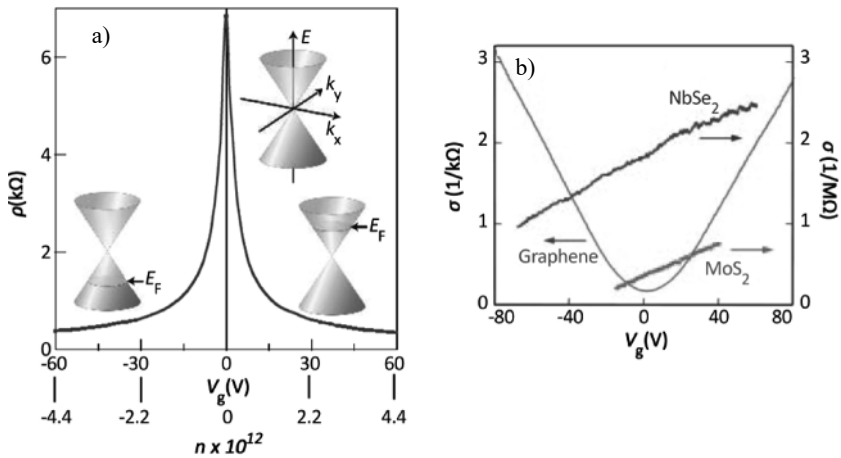

Figure 1.24. *Resistivity variations of graphene and two 2D materials as a function of gate potential (Vg) and charge densities*

COMMENT ON FIGURE 1.24.– *a) Resistivity ρ of a graphene sheet inserted as a channel in a field effect transistor subjected to a gate potential V_g. The perfect symmetry of the curve $\rho_{xx} = f(V_g)$ with respect to the axis $V_g = 0$ V corresponds to completely pure graphene and is obtained at very low temperatures. Note that for a gate voltage and a charge density of zero, graphene maintains a finite resistivity value of around 7 kΩ. The different conductivity regions are shown alongside energy band diagrams and the Fermi level (E_F) corresponding to each polarization;*

the negative and positive values of n correspond to holes and electrons, respectively. With the device used here, the density of charge carriers in electrons or holes varies linearly as a function of voltage, according to $n = \alpha V_g$ *where* $\alpha = 7.2\times10^{10}\ cm^{-2}V^{-1}$. *Adapted from Geim and Novoselov [GEI 07]. b) Comparative conductivity curves of graphene and two 2D semiconductors,* MoS_2 *and* $NbSe_2$. *Adapted from [NOV 05b].*

Using a FET and placing the graphene (FET channel) above a "trench" made in the gate dielectric (SiO_2), Bolotin *et al.* [BOL 08a] were able to show that the electrical properties of graphene are closely linked to the preparation method and are highly sensitive to the possible presence of impurities, which may simply result from contact with the support. The conduction and mobility curves (Figures 1.25a and 1.25b) show a significant increase in these two quantities following thermal treatment.

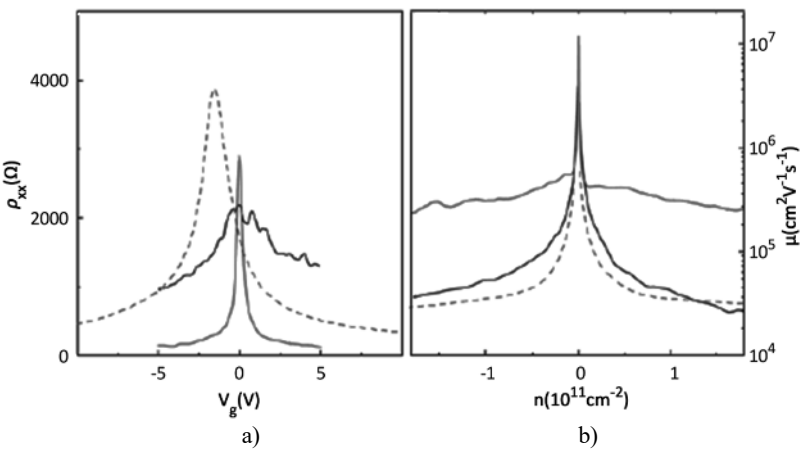

Figure 1.25. *Resistivity of graphene and mobility of charge carriers*

COMMENT ON FIGURE 1.25.– *a) Variation of resistivity* ρ_{xx} *as a function of* V_g *(gate potential). The variation curves obtained before and after heat treatment are shown in blue and red, respectively. The dotted line shows the variation curve for a standard graphene fragment. b) Variation of mobility* μ *as a function of charge densities, before (blue) and after (red) heat treatment. Adapted from [BOL 08b].*

This indicates that the very high mobility values of over 150000 cm^2/Vs cited in the literature can only be obtained for extremely pure graphene. These values correspond to ballistic-type charge transport mechanism, for which the mean free path is of the order of 1 μ. Mobility values for untreated graphene are much lower

(around 15000 cm^2/Vs) and the transport mechanism which occurs in this case is partially dependent on diffusion; the mean free path of the charges is also smaller, at around 150 nm [BOL 08a][22].

1.5.2. *Graphene production techniques*

Several techniques have been developed for producing graphene on a commercial scale. Notable examples include the CVD method developed in 2008–2009 and the chemical and electrochemical exfoliation methods [PAT 14], which are less costly than CVD but which produce lower quality graphene.

One technique involves growing graphene epitaxially on a SiC crystal, under atmospheric argon pressure and at high temperature (1650°C). This particular technique eliminates graphene transfer operations and thus makes it possible to obtain a graphene film of the same size as the crystal, deposited directly on an insulating support; these properties are essential for the creation of FETs [EMT 09].

1.5.2.1. *CVD on a solid catalyst*

The first graphene deposits obtained using the CVD technique were made on mono- or poly-crystalline nickel and copper substrates. In both cases, a gaseous stream of methane and hydrogen heated to about 900°C–1000°C was used; this gaseous mixture decomposes on contact with nickel or copper, releasing carbon atoms. Variations of both processes have also been developed, essentially involving modifications to the gas flow rate and to the proportions used in the CH_4/H_2 mixture [ZHA 13]. Note that formation conditions using CVD are similar to those used for CNTs; the only differences relate to the nature of the catalyst and the higher temperatures used.

1.5.2.1.1. Graphene deposition on nickel

The fact that CVD can be used to form thick graphitic deposits on solid nickel substrates is a well-known process, which was adapted by Kim *et al.* [KIM 09] to obtain graphene monolayers. The authors replaced the solid nickel with a very thin film (300 nm), heated to about 1000°C, over which a mixture of methane and hydrogen flows. As the methane dissociates, carbon atoms are released, and these then solubilize inside the nickel; on cooling, the atoms re-diffuse on the surface and

22 For the majority of the most conductive materials, the mean free path, which depends on the applied electric field, is between a few nm and a few tens of nm. The mean free path of copper, for instance, is around 40 nm [GAL 16].

recombine to produce a highly homogeneous monolayer of graphene film (Figures 1.26a and 1.26b).

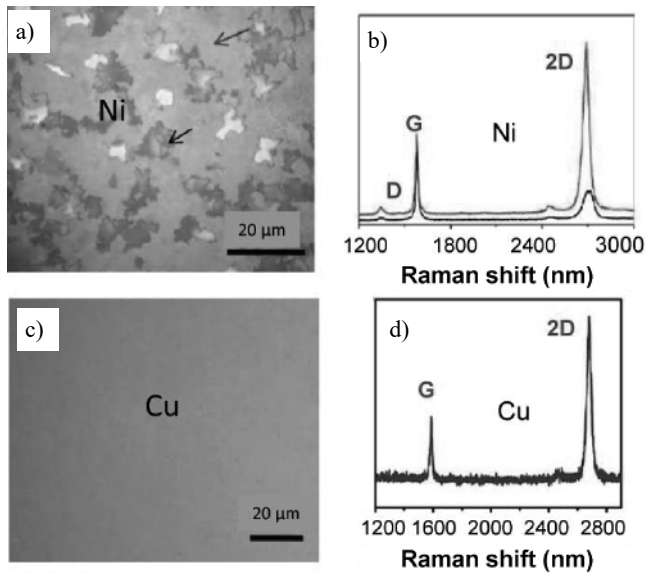

Figure 1.26. *Graphene deposits obtained on Ni and Cu substrates, transferred to a Si/SiO_2 substrate*

COMMENT ON FIGURE 1.26.– *a), c) Optical images of graphene fragments deposited on Ni and Cu, respectively. Note the homogeneity of the graphene film obtained on Cu in contrast with the deposits on a Ni substrate. b), d) Raman emission spectra of graphene for the two deposits. b) In the case of nickel, the heterogeneity of the deposit (fragments indicated by black and red arrows in image a) results in two distinct Raman spectra; the red spectrum corresponds to a monolayer of graphene with some defects (non-zero D band around 1300 cm^{-1}), while the spectrum shown in black corresponds to a multilayer deposit (characterized by a very low-intensity of 2D band). The perfect homogeneity of the graphene film obtained on copper is confirmed by the presence of the two characteristic 2D and G bands alone, with an intensity ratio I_{2D}/I_G of almost exactly 2; this is characteristic of a monolayer graphene film. Adapted from [ZHA 13].*

According to the authors, graphene formation is promoted by the small number of carbon atoms dissolved in the nickel film and by the fact that the lattice of nickel atoms (111) is, in geometric terms, highly compatible with the graphene lattice.

Single-crystal Ni must be used in order to obtain graphene of homogeneous thickness. Polycrystalline nickel features more grain boundaries, resulting in more homogeneity defects in the form of multiple layers along the grain boundaries in the metal; these can be seen in the respective Raman spectra[23].

1.5.2.1.2. Graphene deposition on copper

The experimental conditions (CH_4, H_2 and temperature) used for copper are similar to those used with nickel [LI 09b]. However, the use of a copper substrate offers considerably greater control over the formation of a monolayer of graphene with a larger surface area (dimensions of around 1 cm) (Figures 1.26c and 1.26d).

This difference is due to the fact that the carbon atoms coming from the dissociation of methane are only weakly soluble in copper; they thus adsorb directly onto the surface of the metal, producing graphene [ZHA 13]. The images in Figures 1.26c and 1.26d clearly show an improvement in the size and homogeneity of the graphene layers when using copper instead of nickel.

1.5.2.2. *CVD on a liquid catalyst*

One new trend in 2D material production methods involves the use of liquid metal catalysts in CVD. Applied to graphene, this approach might improve its quality. The technique described in detail by Zeng *et al.* [ZEN 14] is comparable to previous CVD techniques, except for the fact that the catalyst is in a liquid state. The carbon atoms resulting from dissociation of the carbon-based precursor (CH_4) are initially dissolved in the molten metal catalyst. The temperature is slowly reduced, leading to a phase change in the catalyst, from liquid to solid surface, and the dissolved carbon atoms then stop diffusing toward the surface. The solidification of the surface limits the concentration of carbon atoms at the surface, thus promoting the development of graphene monolayers; this result has been observed experimentally (Figure 1.27).

23 Different graphene films (G, 2D and D) have different Raman emission bands, meaning that it is possible to assess their thickness and the presence or absence of defects. A monolayer of graphene is characterized by an intensity ratio of approximately 2 between the I_{2D}/I_G bands. Thickness (in terms of the number n of layers) can be measured from the position of the G band, which verifies the wave number relation $\omega_G = 1581.6 + 11/(1 + n^{1.6})$ cm^{-1}. The D band appears only when there are defects present in the graphene, and is located around 1300 cm^{-1}. The 2D band, sometimes considered as a harmonic of the D band, is particularly intense for monolayer graphene and is located at 2750 cm^{-1}. The band decreases in intensity and widens as the number of graphene layers increases [MAL 09, WAL 11].

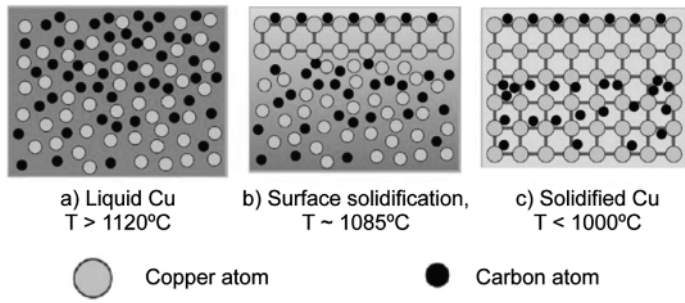

Figure 1.27. *Different steps in the catalytic process leading to a graphene monolayer*

COMMENT ON FIGURE 1.27.– *a) Copper in liquid state with carbon atoms in solution. b) Initial cooling causes surface crystallization of the copper, preventing C atoms in the core of the liquid from diffusing to the surface and thus maintaining a monolayer of carbon deposits on the copper surface, leading to graphene. c) Further cooling keeps the graphene monolayer on the copper surface. Adapted from [ZEN 14].*

In the case of copper, the CVD reaction lasts around 30 minutes at 1120°C; cooling is then progressively applied at the rate of 20°C per minute while maintaining a gas stream of a H_2/CH_4 mixture with a flow rate proportion of 300:6 sccm (standard cubic centimeters per minute). Other metals such as indium or gallium can also be used to synthesize graphene under similar conditions.

The technique can be used to produce homogeneous graphene monolayers of large dimensions. This results from the fact that isotropic graphene grains (IGG) form on the molten copper, and, due to their high mobility, have the ability to react together, with the addition of carbon atoms coming from the precursor, while still respecting the hexagonal geometry of graphene (Figure 1.28).

Remarkably, the charge carrier mobilities measured both intra- and inter-grain are approximately the same (around 3000 cm^2/Vs); this confirms the homogeneity of graphene after the coalescence of two IGGs. The coalescence of large numbers of grains results in dimensions of almost 1 cm^2; this constitutes significant progress toward obtaining large surfaces of high-quality graphene. This method is promising in terms of wider applicability, and may also be used for controlled synthesis of other 2D materials [ZEN 18].

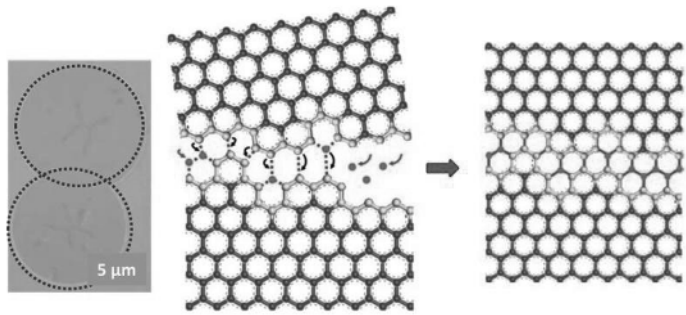

Figure 1.28. *Formation of a single layer of graphene by "joining" two graphene grains (IGG). a) Optical image of two partially overlapping IGGs. b) Formation of –C–C– bonds between the two IGGs with the addition of carbon atoms (in red). c) A single layer of graphene is obtained when the IGGs interconnect. Adapted from [ZEN 16]*

1.5.2.3. *CVD for large-scale production*

Given the strategic importance of graphene, several improvements to the CVD process have been suggested over the last few years, aimed at increasing the scale and lowering the cost of graphene production. CVD is the only known process which is suitable for large-scale graphene production, insofar as the two successive operations involved in synthesizing graphene and transferring it onto a flexible support can be carried out in a continuous and automated manner.

One notable example is the adaptation of the roll-to-roll or "R2R" printing process for producing graphene in the form of films measuring 30 cm wide and several meters long. Research in this area has received significant financial support from industrial groups and is the driving force behind a number of university-industry consortiums[24].

Several variants of the CVD process used in R2R technology have been put forward in recent years, as described by Xin *et al.* [XIN 18]. This technique has been used to produce large graphene films on a flexible, transparent plastic support. Products of this type, which are essentially equivalent to transparent and mechanically flexible metallic electrodes, may be used in a wide range of applications; notable examples include photovoltaics, the production of large organic light-emitting diodes (OLEDs), opto-electronic sensors and, more generally, a whole range of portable and flexible electronic and photoelectronic devices [XIN 18].

24 The European Union has provided funding for a consortium of universities and industrial actors aimed at developing large-scale graphene production techniques.

Three major CVD processes which are compatible with the R2R technique have been developed for large-scale production of graphene on copper substrates. These include atmospheric pressure CVD (APCVD) [VLA 13], low pressure CVD (LPCVD) [KOB 13] and plasma-enhanced CVD (PECVD) [YAM 13] and mostly involve the use of a copper ribbon as catalyst. APCVD is the easiest of the three processes to implement and also produces the lowest quality of graphene [XIN 18].

The second step in the graphene synthesis process consists of detaching the graphene from the copper ribbon and transferring it to a transparent, flexible plastic support. Several different methods have been proposed for carrying out this operation in a continuous manner. One consists of hot-pressing the Cu/graphene film onto an adhesive plastic tape, then using chemical or electrochemical techniques to strip away the copper. The result is a composite graphene/plastic film with electrical conduction and optical transmission characteristics comparable to those of ITO (indium tin oxide) electrodes, with the added advantage of high mechanical flexibility in comparison with ITO.

Bae *et al.* [BAE 10], working in collaboration with Samsung, were among the first to produce hybrid rolls of graphene bonded to plastic, almost 1 m in length, using the R2R technique. Later, Kobayashi *et al.* [KOB 13], working for Sony, succeeded in producing graphene films of over 100 m in length, with a quality comparable to that of ITO plates, using this method (Figure 1.29).

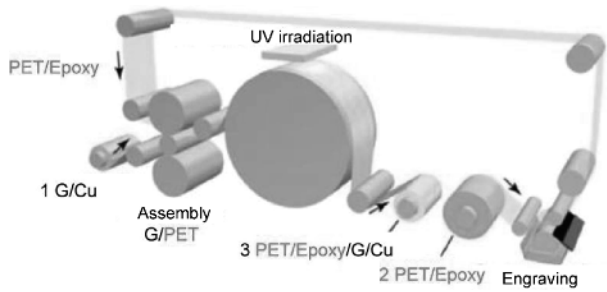

Figure 1.29. *Steps in continuous tape formation [PET/epoxy/G/Cu]*

COMMENT ON FIGURE 1.29.– *The first tape (PET + epoxy) is etched, then is brought into contact with the graphene-on-copper tape [G/Cu]. UV irradiation of the epoxy creates adhesion between the graphene and the PET, creating a [PET/epoxy/graphene/Cu] tape which is then wound onto a spool. The second step (not shown in the figure) is to unwind the composite film in a copper etching bath (acid solution), followed by various rinsing and drying operations needed*

to produce the final PET/G coil. The PET/G tape displacement speed is around 10 cm/minute. Adapted from [KOB 13].

Kobayashi *et al.* [KOB 13] used copper tape, heated to around 1000°C using the Joule effect, which passes slowly through a chamber in which a gaseous mixture of methane and hydrogen was made to circulate at reduced pressure. Precise regulation of the gas flow and the copper tape feed speed was essential in order to obtain a high-quality monolayer graphene film.

Once the graphene film has been formed, a further continuous process is used to transfer it onto a plastic substrate. This is done by bringing the [graphene/Cu] tape into contact with a thermo-adhesive tape formed from a combination of PET (polyethylene terephthalate) and epoxy, which becomes adhesive under UV radiation; this initially produces a hybrid [Cu/graphene/epoxy/PET] tape. This tape is passed through an acid solution (to dissolve the copper), rinsed with water and then dried to produce a graphene film on a plastic substrate. Graphene prepared in this way (a tape of 100 m length and 20 cm wide, supplied in coil form) is characterized by a square resistance of between 150 and 250 ohms/sq and by an optical transmittance of around 85% [KOB 13].

This conductivity is significantly lower than that of extra-pure graphene, but can be improved by depositing metallic silver nanowires on the PET tape. In this case, the square resistance is less than 10 Ω; the optical transmittance value remains very high, of the same order of magnitude as before [DEN 15a].

1.5.2.4. *Chemical techniques for reduced graphene oxide (r-GO) production*

The starting material used in r-GO production is graphite oxide, which may be considered to be a multi-layered precursor for GO. A wide variety of graphite oxidation methods have been described. One of the oldest, which is still widely used, is the Hummers method, which consists of oxidizing graphite powder with potassium permanganate[25]. Exfoliation is then carried out using strong ultrasonic agitation in a liquid medium; the whole operation takes around an hour [EIG 13].

The chemical reaction described by Hummers results in significant degradation of the crystal lattice, as C–C bonds break down, following oxidation and the release of CO_2. The number of defects can be reduced by carrying out the operation at low

25 Hummers' method consists of gradually adding potassium permanganate to graphite powder suspended in a solution of silver nitrate and sulfuric acid. The reaction is exothermic and can become explosive if the temperature is not controlled [HUM 58]. Starting with 1 g of graphite powder, Eigler *et al.* [EIG 13] were able to obtain 500 mg of GO and 200 mg of graphene following chemical reduction.

temperatures, limiting the release of CO_2, bond breakage and the appearance of structural defects [EIG 13].

Once GO has been obtained, in the form of a suspension in a water-alcohol mixture (0.1 mg/mL), the GO is dispersed onto a solid support, then reduced using a mixture of hydroiodic acid (IH) and trifluoroacetic acid (CF_3CO_2H) in vapor form to produce reduced graphene, r-GO, in the form of flakes of between 500 nm and 1 µm in size[26]. Statistical Raman analysis of these r-GO flakes shows that after reduction, they can be classified into three distinct fractions based on the full width at half maximum (FWHM) of the 2D Raman band centered on 2700 cm^{-1}. These fractions are: (1) r-GOs with low structural defect densities (30 cm^{-1} < FWHM < 40 cm^{-1}); (2) r-GOs of "average" quality (40 cm^{-1} < FWHM < 50 cm^{-1}); and (3) a high proportion of r-GOs with large numbers of structural defects (FWHM > 50 cm^{-1}) (Figure 1.30).

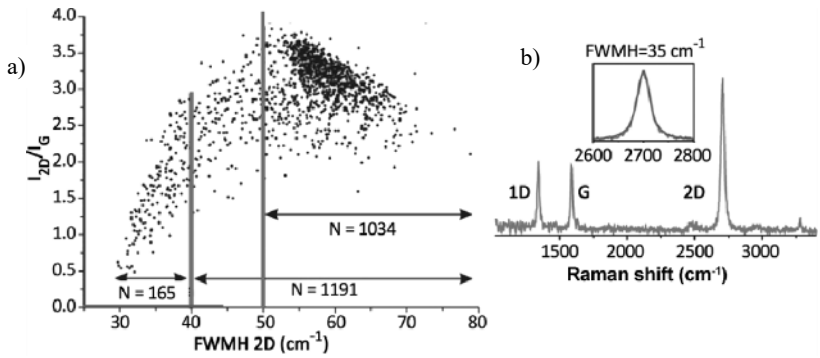

Figure 1.30. *Statistical evaluation of the quality of graphene obtained by GO reduction and adsorbed on Si/SiO_2*

COMMENT ON FIGURE 1.30.– *a) Statistical distribution of observed Raman spectra at different points on the surface and as a function of the width (FWHM) of the 2D scattering line centered at ~2700 cm^{-1} and of the I_{2D}/I_G ratio. The 165 spectra for which FWHM (at 2700 cm^{-1}) < 40 cm^{-1} correspond to graphene with very few defects; 1034 correspond to graphene with a high density of structural defects (FWHM > 50 cm^{-1}) and 157 are of medium quality (40 < FWHM < 50 cm^{-1}). b) Raman spectrum of a graphene flake with low defect density (FWHM ~ 35 cm^{-1}). Adapted from [EIG 13].*

26 Hydroiodic acid and trifluoroacetic acid offer non-toxic alternatives to hydrazine as GO reduction agents.

From these considerations, it appears that graphene obtained by GO reduction is not as pure as graphene obtained by mechanical exfoliation or by CVD. Nevertheless, although the conduction properties of this graphene are inferior, the fact that it can be produced at low cost with no need for heavy material investments represents a significant advantage. Furthermore, the mechanical and conductive properties of even "inferior" graphene are sufficient for many applications.

More recently, Cheng *et al.* [CHE 16] developed an original method for obtaining bulk (multilayer) graphene by laser irradiation of a GO aerogel[27], a reduction technique developed a few years earlier by Kaner and coworkers [STR 12]. The authors used this technique to obtain a variety of graphene which is exceptionally well suited for use in battery electrodes. The method is particularly striking because of the way laser irradiation (1 watt power) from a single point in the aerogel results in the transformation of the whole aerogel into bulk graphene (Figure 1.31).

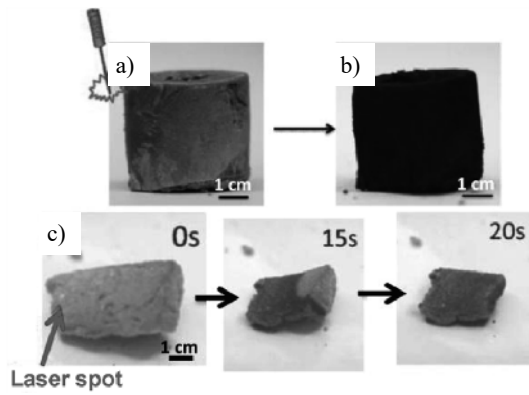

Figure 1.31. *Transformation of GO bulk aerogel into graphene by point laser irradiation. a) GO aerogel before transformation. b) Reduced graphene after transformation. c) Optical photographs showing the gradual and complete transformation of a GO aerogel sample (light gray) to graphene (dark gray) between 0 and 20 seconds. Adapted from [CHE 16]*

A transformation of this type, starting from a single point in the material, is only observed when the GO is in aerogel form; this differs from "conventional" GO in that pockets of air and water are trapped within the carbon network. The authors found that the impact of the laser beam results in localized GO reduction with the

27 GO aerogel is obtained by flash-cooling a suspension of GO in water (5 mg/ml) and drying it in a freeze dryer.

release of CO, CO_2 and H_2O; a variety of carbon-based fragments, such as $C_6H_4^+$ and $C_4H_2O_4^{2+}$, are also produced. These fragments (identified by mass spectrometry) react with the oxygen present in the aerogel, producing a significant amount of heat; this heat is sufficient to trigger local dissociation of new fragments and the removal of oxygen groups, thus triggering an uninterrupted propagation of the reduction reaction throughout the whole volume of the material. The result is a block of reduced graphene which retains the form and volume of the original material.

An added advantage of this technique is that it can be used to produce bulk graphene doped with various hetero-elements such as N, S, P and Pt. This is done by mixing chemical compounds containing the corresponding atoms with the GO suspension; during irradiation, the compounds are degraded and release these atoms, which are then implanted in the graphene [CHE 16].

The same authors have suggested similar strategies for producing highly porous graphene foams with innovative elastic properties [LV 16]. These foams are obtained using a suspension of GO, to which SDS (sodium dodecyl sulfate) then Nonidet P40 (4-nonylphenyl-polyethylene glycol) are added under strong agitation. SDS promotes the formation of air bubbles around the GO sheets, while Nonidet P40 acts as a solidifying agent when the solution is freeze-dried[28]. With the addition of these two surfactants, the solution turns from black to gray in color, and significantly increases in volume; the authors explain this due to the presence of air bubbles which agglomerate around the GO particles (Figure 1.32b).

Freeze-drying the solution produces a gray foam, which is then heated to 200°C for 1 hour to complete solidification; a subsequent heating to 1000°C in argon for 2 hours eliminates the surfactants and reduces the oxide to a solidified graphene foam (SGF) which is black in color and is smaller in size than the foam obtained after freeze-drying (Figure 1.32).

The resulting foam is extremely elastic, and these properties are perfectly conserved over repeated cycles (1000 cycles) of compression and relaxation of 80% in the axial direction. The authors state that their foam performs much better in this respect than the vast majority of known foam materials. The mechanical properties of the foam are closely linked to the ratio of the two surfactants used, along with the annealing temperature. The elasticity modulus E and the conductivity σ are optimized using an annealing temperature of 1000°C, where E = 292 kPa and $\sigma = 55.2$ S m^{-1} [LV 16].

28 The graphene oxide solution is freeze-dried by freezing the solution in liquid nitrogen, then vacuum drying by ice sublimation for 72 hours.

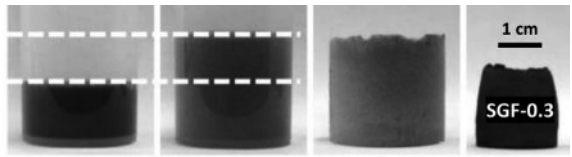

Figure 1.32. *Different stages in the production of solidified graphene foam, SGF*

COMMENT ON FIGURE 1.32.– *a) GO suspension before addition of surfactants. b) Volume increase of GO suspension after the addition of surfactants (under strong agitation). c) Solid GO foam obtained after freeze-drying. d) Solidified graphene foam, SGF-0.3, after heat treatment. 0.3 refers to the amount of Nonidet P40 introduced into the GO solution (0.3 ml). Adapted from the Supporting Information for [LV 16].*

1.5.3. *Applications of graphene and graphene derivatives*

The exceptional mechanical, electrical and thermal properties of a graphene monolayer were discovered not long after the material itself. In addition to its low mass density (2.26 g cm^{-3}), its mechanical characteristics include a tensile strength of 130 GPa and an elasticity modulus E of 1100 GPa; in comparison, stainless steel has an elasticity modulus E of around 200 GPa and a tensile strength of approximately 0.5 GPa. The electrical conductivity of a graphene monolayer (10^8 S m^{-1}) is higher than that of metals such as copper (6×10^7 S m^{-1}), and a graphene monolayer is able to withstand current densities of up to 10^{10}–10^{11} A m^{-2} without damage. Its thermal conduction properties are also excellent, with a maximum recorded value of 5300 Wm^{-1} K^{-1}, compared to 400 Wm^{-1} K^{-1} for copper. Evidently, these values only hold for extremely pure, defect-free graphene. The graphene produced for large-scale operations does not perform at this level; however, the properties of this "average" graphene are sufficient in many cases. It is helpful to establish clear requirements in terms of the quality, uniformity and reliability of graphene required for particular applications, in order to create products and devices which are able to compete with existing systems in terms of both cost and performance[29].

29 The Manchester GEIC (Graphene Engineering and Innovation Centre) website, along with that of the Graphene Council, was created in 2013 for the development and exploitation of graphene and provides a general idea of the many present and future applications of graphene material in various forms. For example, the interview with T. Barkan (Graphene Council) on "The future of graphene", published in February 2019, is particularly informative (AZOnano, https://www.azonano.com/article.aspx?ArticleID=5135).

For instance, the quality of graphene used in the form of multilayered sheets to produce electrode materials, used in solar energy conversion devices or for energy storage in the form of various battery systems, is not of critical importance. The same is true of fibers designed for use as electric cables.

Graphene has many actual and possible applications in the fields of energy, electronics and medicine. A small selection of products derived from graphene and GO, available in various forms (paper, fibers, tape, etc.), will be described below, along with some specific applications relating to polymer-graphene or polymer-GO composites. Graphene nanofragments, known as graphene quantum dots (GQD), will be discussed separately as their specific properties are very different from those of graphene and of CDs.

1.5.3.1. *Graphene oxide*

Graphene oxide, obtained by oxidizing graphite using the Hummers method, takes the form of a lamellar product consisting of a stack of graphene sheets, functionalized in the plane and periphery by oxygenated groups (carboxylic on the edges, phenolic and epoxydic in the plane). Sheets are exfoliated by ultrasound stirring in an aqueous medium, creating a colloidal suspension of GO nanosheets in water. These nanosheets are around 1 nm thick, with lateral dimensions varying between a few nm and several hundred microns (Figure 1.33).

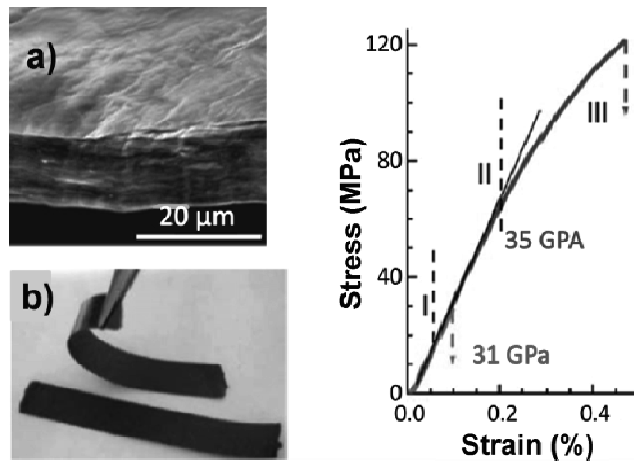

Figure 1.33. *Mechanical characteristics of a film of graphene oxide (GO)*

COMMENT ON FIGURE 1.33.– *a) SEM image of a GO film approximately 10 µm thick. b) Folding a GO tape approximately 25 µm thick. c) Stress/strain curve of a*

GO film 5.2 µm thick. The regions labeled I, II and III correspond to strictly elastic, quasi-elastic and plastic variations, respectively. The red curve shows a first variation in strain (with elasticity modulus E of 31 GPa) while the blue curve corresponds to the second deformation cycle (with E = 35 GPa). Adapted from [DIK 07].

The suspension is filtered very slowly through a porous disk, producing a thick, compact film after about 12 hours. The thickness of this film can vary from 1 to 30 µm, depending on the quantity of solution used. The resulting paper-like product has very good mechanical properties due to strong interactions between hydroxyl groups. For films of a few µm thickness, the elasticity modulus (E) is around 30 GPa [DIK 07].

According to the authors, the fact that the elasticity modulus of the GO increases with the application of several stress/strain cycles is evidence of an axial realignment of GO fragments, leading to increased rigidity. Although the elasticity modulus of GO varies in a non-negligible manner according to the method used to produce it, it remains high, much higher than the elasticity modulus of similar papers resulting from the agglomeration of CNT (buckypaper: ~7 GPa), or of inorganic lamellar compounds such as vermulite (E ~12 GPa). Its tensile strength, σ, is also high (between 38 and 125 MPa); this value is higher than that of buckypaper (between 10 and 75 MPa) and comparable to that of a vermulite paper (between 25 and 150 MPa). These mechanical properties outperform those of many materials; however, the mechanical characteristics of a graphene monolayer are still higher (E ~1 TPa and σ ~130 GPa) [DIK 07].

The presence of ionizable carboxyl groups (hydrophilic) on the periphery of the NPs and of large graphitic domains (hydrophobic), along with some epoxy and phenolic groups, in the plane of the GO sheets means that the material is amphiphilic and possesses tensioactive properties. For this reason, it can be used as a dispersing agent in water for highly hydrophobic products, such as CNTs. This amphiphilic property is also the reason why GO sheets adhere to gas bubbles (N_2, CO_2) and can migrate to the liquid-air separation surface, forming a compact layer, which can then be transferred to a solid support using the Langmuir-Blodgett technique. The hydrophilic properties of the material may also be increased by increasing the alkalinity of the medium, promoting the ionization of the carboxyl groups into carboxylates; in this case, the amphiphilic character decreases [KIM 12] (Figure 1.34).

The amphiphilic properties of GO sheets make them suitable for a wide range of applications. A GO sheet may be seen as a 2D di-block copolymer with, on one side, a strongly hydrophobic graphitic block and, on the other side, a strongly hydrophilic

carboxylic block. The amphiphilicity of the sheet can be used to improve the crystal order of another polymer interacting with the GO.

A result of this type occurs when a conductive polymer such as poly(3,4-ethylenedioxythiophene): poly(styrene sulfonate) (PEDOT-PSS) is mixed with non-conductive GO sheets. Instead of the expected decrease in conductivity, this value increases by a factor of 10, and a highly viscous, gel-like adhesive product is obtained. This seemingly paradoxical effect results from improved organization of the PEDOT chains, induced by contact with the GO sheets [TUN 11].

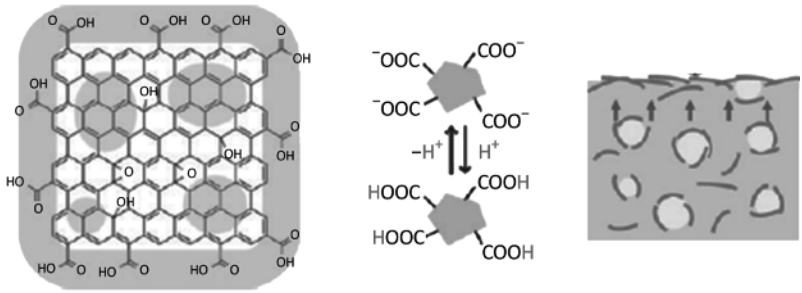

a) b) c)

Figure 1.34. *Graphene oxide (GO) sheets*

COMMENT ON FIGURE 1.34.– *a) Distribution of oxygenated functional groups on the surface of a GO sheet (green: hydrophobic graphitic regions, yellow: hydrophilic carboxylic regions). b) Ionization of COOH groups and increase in the hydrophilicity of GO as pH increases. c) Adsorption of GO sheets on the surface of gas bubbles (yellow) and migration to the water/air interface. Adapted from [KIM 12].*

Finally, an important property of GO suspensions is their ability to organize and form liquid crystals. This property has been demonstrated by several authors [KIM 11, XU 11], and is useful for many applications, including large-scale fabrication of graphene fibers (GFs) (see section 1.5.3.3).

1.5.3.2. *Graphene paper: a semi-metallic r-GO sheet obtained after reduction of graphene oxide*

The technique used to create GO films from suspensions in water using filtration has also been adapted for the production of graphene films. This approach, developed by Chen *et al.* [CHE 08], consists of reducing a suspension of GO using hydrazine; following vacuum filtration, this produces metallic-like films of controllable thickness (from a few tens of nm to several microns) (Figure 1.35).

These “paper” sheets obtained through GO reduction may be assimilated to a variety of graphene noted r-GO. This material exhibits high mechanical resistance and good electrical conductivity, and this latter characteristic differentiates it from GO, which is an insulator.

The mechanical and electrical properties of graphene paper are strongly dependent on the strength of the cohesion established between graphene sheets. This cohesion may be weakened by the presence of residual gases and liquids left over from previous chemical treatments. Located between the sheets, these residues are difficult to remove due to the impermeability of the material. An American team has recently managed to solve this problem by creating holes on the surface of the graphene sheets (making “holey graphene” , noted h-graphene) in order to evacuate impurities, then using a heat treatment to rebuild the hexagonal structure of the graphene mesh.

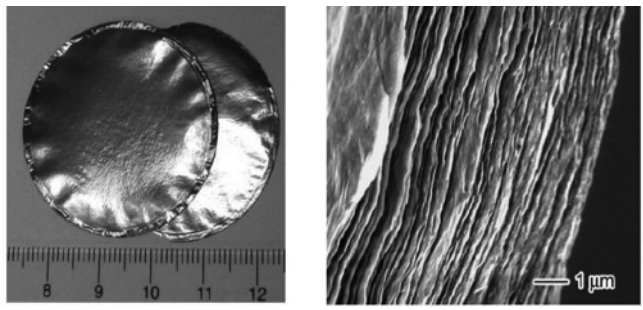

a) b)

Figure 1.35. *Graphene paper (r-GO) obtained after reduction of graphene oxide (GO) sheets. a) Photograph of two metallic graphene sheets (front and back views). b) Scanning electron microscopy (SEM) image of a graphene paper sheet showing stacked sheets of graphene. Adapted from Chen et al. [CHE 08]*

This method, described by Chen *et al.* [CHE 19], consists of heating graphene sheets in air over a long period (10 hours at 700 K); this results in a porous structure, with holes in the graphene sheet of approximately 15 nm in diameter (Figure 1.36a).

Treating the h-graphene obtained in this way in an inert atmosphere and at very high temperatures, using the Joule effect (2700–3000 K), the crystalline structure of the graphene is restored; this is confirmed by the Raman spectra (Figure 1.36b).

Reprocessed h-graphene exhibits very good electrical and thermal properties. The conductivity of the graphene sheets increases from 128 S cm^{-1} before treatment to 2209 S cm^{-1} after treatment at 2700 K; similarly, the mobility of the charge

carriers increases from 26 $cm^2 V^{-1}s^{-1}$ to 673 $cm^2 V^{-1}s^{-1}$. Paradoxically, the density of charge carriers after reconditioning is lower than that observed in h-graphene (2.18×10^{19} cm^{-3} compared to 3.3×10^{19} cm^{-3} before restoration of the graphene structure); this signifies that treatment at 2700 K has the effect of removing the defects and impurities present in h-graphene which are responsible for weakened conductivity [CHE 19].

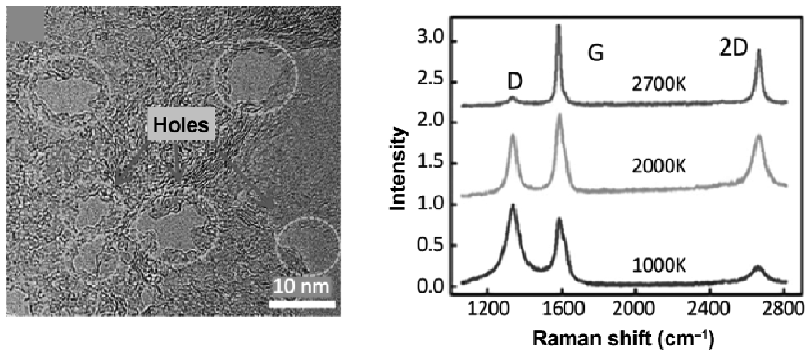

a) b)

Figure 1.36. *Reprocessed h-graphene*

COMMENT ON FIGURE 1.36.– *a) High-resolution transmission electron microscopy (HRTEM) image of a graphene sheet with multiple perforations (circled in green) created by air heating (h-graphene). b) Raman spectra of h-graphene sheets reconditioned at different temperatures. Only heat treatment at very high temperature (2,700 K) produces a defect-free graphene, as we see from the very low intensity of the D-band. Adapted from [CHE 19].*

Thermal conductivity is also greatly improved, increasing by a factor of 7 up to 863 $Wm^{-1}K^{-1}$ after treatment at 2700 K; this corresponds to a thermal conductivity more than twice that of copper. These thermal and electrical properties far exceed the known characteristics of graphene sheets, suggesting new potential applications for this type of material in the field of electronics and energy, including the development of new electrode materials.

Another feature of r-GO films is their impermeability to gases, liquids and many aggressive chemical species, such as hydrofluoric acid. This property is only effective if the r-GO films are free from structural defects (holes); one of the methods that seems to be most effective in producing non-porous r-GO is to reduce the GO using hydroiodic acid or ascorbic acid (vitamin C) [SU 14].

Impermeability is a particularly useful property for protecting organic electronic devices against humidity; these devices are usually encapsulated in PET (polyethylene terephthalate) films covered with a thin layer of aluminum. Su *et al.* [SU 14] have shown that an optically transparent 30 nm r-GO film, obtained by reducing GO with hydroiodic acid (HI), is almost completely impermeable to hydrogen and water vapor; the water permeation rate through a membrane of this type is around 10 mg m^{-2} day^{-1}, 100 times lower than the value for "standard" protection (aluminum-coated PET membrane).

In this, r-GO film differs from GO film, which exhibits abnormally high water permeability, which can also be controlled electrically [ZHO 18]. A further advantage of r-GO is that it is biocompatible, meaning that it can be used in the biomedical field for designing biosensors.

1.5.3.3. *Graphene fibers*

Qu and coworkers were among the first to propose a method for large-scale GF production using an easy and inexpensive approach, based on a suspension of GO in water [DON 12]. This method is very simple, consisting of heat treating a suspension of GO (8 mg GO/ml) in a glass tube (inner diameter 0.4 mm), closed at both ends, at 230°C for 2 hours. This leads to a fiber with a diameter of 150 µm when wet, reduced to 35 µm after drying.

From a mechanical perspective, the stress/strain variation curves improve significantly following treatment at 800°C for 2 hours in argon, increasing the tensile strength from 120 to 420 MPa. The electrical conductivity of these fibers is around 10 S/cm, a value which is comparable to that of fibers made from CNT; it remains stable after over 1000 repetitive bending/relaxation cycles. These fibers can also be knotted or twisted, showing their exceptional flexibility (Figure 1.37).

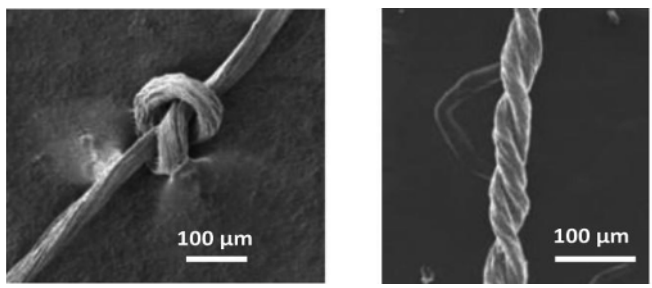

a) b)

Figure 1.37. *SEM images of graphene fibers. a) Knotted fiber. b) Twisted two-strand graphene fiber. Adapted from [DON 12]*

These fibers can be given new properties by doping with inorganic compounds. For example, incorporating a semiconductor such as titanium oxide (TiO_2) into the initial GO solution results in the creation of a photoelectronic device in which the GF generates an electrical response when subjected to a photon pulse. The addition of ferric oxide, Fe_3O_4, to the GO suspension produces a "magnetic" GF, which moves or bends elastically when held near a magnet [DON 12].

Given the technological importance of these fibers, they are a subject of active research, with many teams attempting to produce GFs with properties as close as possible to those of pure single-layer graphene films. We recall a graphene film which is mechanically exfoliated from a graphite crystal has an elasticity modulus of ~ 1 TPa, tensile strength of 130 GPa, electrical conductivity of 10^8 S/m with an ampacity of 10^{12}–10^{13} A/m^2 and thermal conductivity of up to 5300 W/mK.

The Gao group was recently able to demonstrate large-scale, continuous production of very high-quality GFs [XU 16]. Their improvements largely concern an improved orientation of the GO sheets, which are always, initially, obtained as a dispersion of GO monolayers in water (from 1 to 10 mg GO/ml solution). This dispersion is then transferred into a solution of N,N dimethyl formamide (DMF), which has the effect of creating a liquid crystal structure, with a parallel arrangement of the GO sheets. This substance is then extruded through a small diameter die (60 μm), then the fiber is unwound by rotating rollers which maintain a slight stress in the GO thread. The resulting GO fiber (GOF) is wound directly into a coil. Heat treatment under nitrogen at 3000°C is used to transform the GOFs into GFs (Figure 1.38). These GFs have very good mechanical properties along with excellent electrical and thermal conductivity. The Young's elasticity modulus is between 385 and 400 GPa (measured using a 5 mm length of wire), and the tensile strength is in the range of 1.8–2.2 GPa. Conductivity at room temperature is up to 0.8×10^6 S/m and is independent of the tested wire length; the ampacity is extremely high and corresponds to current densities of 2.3×10^{10} A/m^2. These values are comparable to, and sometimes better than, those measured with wires formed from CNTs.

The possibility of producing extremely flexible, mechanically strong GFs with electrical properties comparable to those of metals such as copper and very low mass densities on a large scale opens up a wide range of possible applications. The authors showed that wound GFs may be used to replace copper wires in electric motors, something which represents a significant advance in terms of mass, considering the differences in density between GF (0.23 g/cm^3) and copper wires (8.96 g/cm^3). Similarly, the high ampacity of GFs could be exploited in producing incandescent lamps which, all other things being equal, would emit light with a higher intensity than that obtained using a tungsten filament [XU 16].

Alongside the work cited above, the same group showed that the conductivity of GFs can be greatly increased by doping with certain elements. Using GFs with a high purity level, prepared according to the method described above, doping agents in the vapor state can be inserted into the fibers: the use of ferric chloride ($FeCl_3$), bromine (Br_2) or potassium (K) results in GFs with conductivities of 0.77×10^7 S/m (GF-$FeCl_3$), 1.5×10^7 S/m (GF-Br_2) and 2.24×10^7 S/m (GF-K), respectively [LIU 16b]. These values come very close to those of copper (~ 6.10^7 S/m at 20°C).

Finally, the same team has recently shown that GFs can become superconductors when doped with calcium, using the same process as before [LIU 17c]. This superconducting property, which is not specific to GFs, has already been observed in different carbon allotropes (diamond, graphite, C_{60} fullerenes, CNT and graphene), but always in very small quantities. In the present case, the authors show that this superconducting property can be obtained in a continuous manner and without limitation along the whole length of a graphene wire, opening up more promising perspectives in terms of applications. The transition to the superconducting state is observed at 11.3 K and becomes complete at 4 K[30]. Remarkably, after transformation, the GF retains its mechanical flexibility when subjected to multiple bending/relaxation cycles.

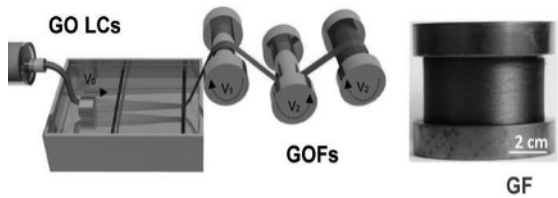

Figure 1.38. *Diagram of the apparatus used in large-scale graphene wire production*

COMMENT ON FIGURE 1.38.– *a) Extrusion of GO in liquid crystal form (GO LC) at speed V_0. The extruded product is subjected to a first heat treatment intended to produce strong agglomeration of the GO particles while maintaining the axial orientation of these particles. Rollers V_1 and V_2 rotate at speeds slightly higher than the extrusion speed V_0, maintaining a slight tension in the extruded fiber. b) A coil of GF obtained after heating the GOF fiber at 3000°C under argon. Note the reflective metallic appearance of the GFs, very different from the yellowish color of GOF yarns. Adapted from [XU 16].*

30 For comparison, commercial NbTi superconducting wire has a transition temperature of 9.7 K.

1.5.3.4. *Graphene-polymer nanocomposites*

The idea of using small amounts of graphene to significantly improve the mechanical, electrical and thermal properties of compositive polymers is attractive. The appeal of graphene as a polymer reinforcement agent, in comparison with other sub-micrometer additives, is its extremely high aspect ratio: this suggests that strong graphene-polymer interactions could be obtained using only small amounts of graphene. Ruoff and his group were the first to exploit this concept, using a suspension of NP-GO in water to develop large-scale composite polymeric materials, consisting of a mixture of polymer and graphene, with significantly improved electrical and mechanical properties [STA 06].

The main difficulty with this process lies in the fact that the graphene nanoparticles (NP-Gs) which must be inserted into the polymer matrix are generally obtained by reduction of NP-GOs which are suspended in water; after reduction, the NP-Gs aggregate immediately, given the hydrophobic character of the NP core. This makes it difficult to insert individual graphene NPs into a polymer solution, particularly considering the fact that most polymers are insoluble in water.

A solution is to make is to make the NP-GO less hydrophilic by chemically treating the graphite oxide with phenyl isocyanate, thus transforming the OH and COOH groups of the graphite oxide sheets into amide and carbamate functions, which are weakly hydrophilic [STA 06]. Exfoliation is not possible in aqueous medium, but is easily achieved in an aprotic solvent such as N,N dimethylformamide (DMF). The authors were thus able to obtain a suspension of functionalized GO NPs (GOf) in an organic medium, one in which many polymers can be solubilized (Figure 1.39).

It is notable that the hydrazine reduction of the NP-GOfs in the presence of a polymer such as polystyrene only results in an aggregation of the graphene NPs with the polymer, and not an aggregation of the NPs themselves; this permits the formation of a graphene/polymer composite (G/P). The transfer of the suspension into alcohol leads to coagulation of the NPs in the form of a grayish powder (Figure 1.39c), which after drying and hot molding under pressure produces black pellets of G/P composites (Figure 1.39d).

The electrical conductivity of the composite is a function of the concentration of graphene NPs by volume, and results from a percolation mechanism that becomes effective at a very low concentration threshold of 0.1%. The conductivity of the composite increases rapidly from 10^{-5} to 0.1 S/m as the volume concentration of the graphene is increased from the percolation threshold up to a concentration of around of 1%. This conductivity value is comparable to that obtained for CNT/polymer composites, but the material is much more cost effective.

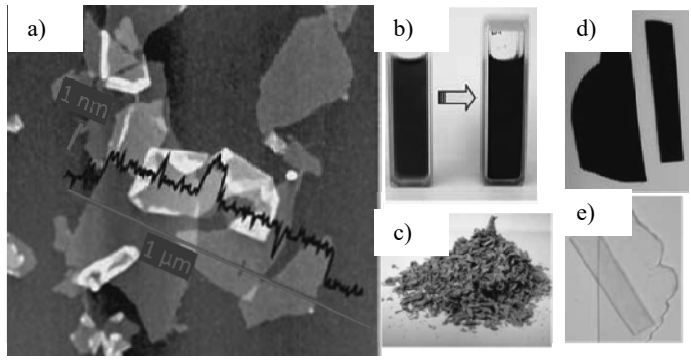

Figure 1.39. *Successive steps in the formation of G/PS composite*

COMMENT ON FIGURE 1.39.– *a) AFM image and profile of functionalized GO nanoparticles (NP-GOf) after reaction with phenyl isocyanate. The NP-GOfs deposited on mica have lateral dimensions of between 1 and a few µm; their thickness, of the order of 1 nm, confirms that monolayer sheets have been obtained. b) Color change (from brown to black) of the NP-GOf suspension in the presence of polystyrene (PS) after reduction with hydrazine and obtention of NP-Gf/PS. (c) NP-Gf/PS powder obtained following coagulation of the suspension in alcohol. (d) and (e) NP-Gf/PS and PS pellets obtained under the same thermal molding conditions. Adapted from [STA 06].*

Since the publication of these first works, which have been abundantly cited in the literature, numerous teams have invested in this research, proposing various improvements and variations to the graphene/polymer composite fabrication process. Several reviews have been published on this subject [POT 11, DAS 13, HU 14, BER 17, MAL 17], which detailing the composites obtained using a wide range of polymers of technological interest, along with variations in production methods, notably techniques for functionalizing graphene NPs; these have led to significant improvements on both mechanical and electronic levels (Figure 1.40).

These new properties have contributed to a vast expansion of the field of application of composite polymers in four essential areas: energy (storage and conversion), biomedical (medical imaging and drug delivery), electronic devices (sensors, transistors, electrodes and electromagnetic shielding) and mechanical development (artificial muscles).

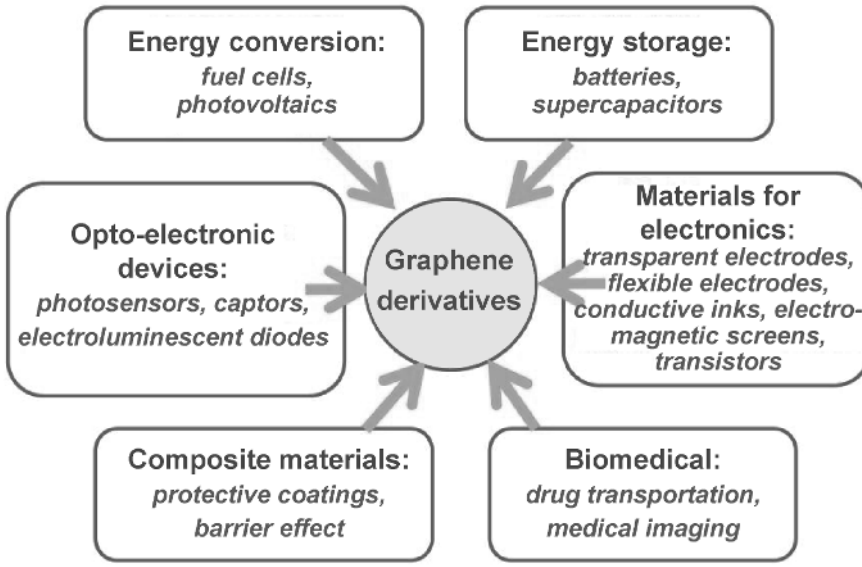

Figure 1.40. *Uses of graphene derivatives in different fields*

1.5.4. *Conclusion*

Graphene is one of the very few materials which combine exceptional electrical and thermal conductivity, the ability to withstand extremely high temperatures and electron current densities higher than those of the most conductive metals (such as copper), mechanical properties (elasticity and tensile strength) which far exceed those of steel and a low mass density (2.3 g/cm^3). However, these properties are only found in almost pure, mechanically exfoliated graphene sheets, which can only be obtained in very small quantities.

CVD techniques have undergone considerable developments, making it possible to produce continuous graphene ribbons of very high quality. However, this technique requires significant material investment and can only be envisaged in an industrial context. The chemical methods used to transform GO into graphene, on the other hand, are more readily available and have also matured in recent years. GO, which can be obtained in large quantities by a simple oxidation treatment of graphite, is the precursor *par excellence* for obtaining large quantities of graphene in various forms. It can take the form of very long fibers of only a few microns in diameter and of very high homogeneity; it may also be used in manufacturing composite materials. The quality of the graphene produced in this way can be considerably improved by a thermal treatment at very high temperatures and in an

inert atmosphere; this has the effect of restoring the graphitic structure of the graphene.

1.6. Graphene quantum dots

GQDs are essentially graphene fragments of nanometric size, and can be assimilated to point NPs (0D) which share the physicochemical characteristics of both graphene and carbon dots (CDs). The quantum confinement effects and edge effects encountered in CDs are expected to be observed in this case, alongside certain properties which are characteristic of the structure of graphene.

GQDs are less than 10 nm in size, and their thickness is less than 10 layers of graphene. They are fluorescent, due to the confinement effect; unlike graphene, GQDs also have a non-zero band gap, meaning that they are semiconductors. This opens up a range of possible applications, for example, in the field of optoelectronics.

1.6.1. *GQD production methods*

Since GQDs were first obtained in 2008 by Ponomarenko *et al.* [PON 08], by fragmenting CNTs, a large number of other techniques have been proposed. These may be grouped into two categories. “Top-down” techniques consist of cutting fullerenes, CNTs, carbon fibers or graphene into fragments, while “bottom-up” techniques aim to synthetize GQDs via a chemical transformation of carbonaceous molecules used as precursors. Citric acid, glucose and a range of other compounds with benzene cores have been used as precursors in GQD production. A detailed description of recent advances may be found in articles such as [TIA 18] and [VAL 17]. For our purposes, we have chosen to present two examples of fabrication methods from the categories cited above.

1.6.1.1 *Top-Down GQD production methods*

One frequently used technique consists of fragmenting a carbon-based material, preferably made up of aromatic nuclei. Graphite is the preferred option, but other materials, such as cotton fibers, have also been processed into GQD using this method [ZUO 17a].

The combined use of microwaves and a chemical treatment of graphite in an acid medium permits the creation of large quantities of GQD and, moreover, does not require significant material investments. This method was used by Luo *et al.* [LUO 16] to obtain emissive GQD films for use in white light diodes (Figure 1.41).

In step 1, a suspension of powdered graphite in a mixture of sulfuric and nitric acid (in proportions of 3:1) is subjected to sonication for 2 hours, then to a microwave treatment at 80°C for 4 hours, leading to the formation of GQD. With average lateral sizes of about 2.5 nm and thicknesses of about 2 nm, corresponding to three to five layers of graphene, these GQDs are characterized by luminescence spectra in the yellow-green range.

In step 2, the GQDs are subjected to further microwave radiation for 12 hours, this time in a strongly basic medium (pH 13) and at a higher temperature (175°C), which has the effect of creating numerous oxygenated and carbonylated groups and removing part of the graphitic structure. These new materials are characterized by a wider fluorescence spectrum that can result in white light-emitting layers. They present a significant advantage over other white light OLEDs (organic light-emitting diodes) in that no multiphase combination of emissive materials is required. However, their luminance value, around 200 candelas/m^2, and their quantitative efficiency of around 0.2% are still modest compared to the performance of current LED lamps.

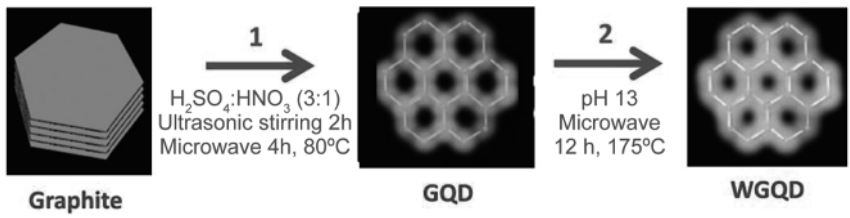

Figure 1.41. *Two-step transformation of graphite into GQDs then into WGQD white luminophores. GQDs emit greenish yellow light, while WGQDs emit white light. Adapted from [LUO 16]*

1.6.1.2. *Bottom-up GQD production methods*

Unlike the previous method, which involved degrading graphitic structural materials, the bottom-up method for GQD production is based on growth reactions using carbon compounds, which, by thermolysis in aqueous medium, are likely to produce condensed aromatic structures. The compounds used as a carbon source may be polycyclic aromatic compounds (pyrene, dinitro 1.5-naphtalene), but non-aromatic compounds, such as citric acid or glucose, may also be used for GQD production.

This technique presents a clear advantage of simplicity in comparison with top-down techniques for obtaining GQDs doped with elements other than carbon. Thus, nitrogen-doped GQDs (N-GQDs) can be obtained in a single step, by directly

treating a mixture made up of a nitrogen derivative and the carbon source compound. N-doped nanomaterials have significantly improved photoluminescence compared to undoped GQDs, and are therefore particularly interesting for medical imaging: in addition to their luminescence properties, they are highly stable in aqueous media and are non-toxic. They also have applications in the energy field and in sensor design [KAU 18].

Gu *et al.* [GU 16] performed thermolysis of citric acid in the presence of ethylene diamine to obtain N-GQDs, with sizes between 5 and 10 nm and thicknesses between 0.8 and 2.5 nm, equivalent to two to five layers. These N-GQDs exhibit a remarkably high internal quantum yield of blue photoluminescence, of the order of 75%, far exceeding the quantum yields usually observed with this type of material.

Another means of obtaining N-GQDs is to start with a single compound, such as 1,3,5-triamino-2,4,6-trinitrobenzene (TATB), including both the carbon and nitrogen atoms needed to form N-GQDs [LI 16c]. A pyrolysis reaction is carried out at high temperatures (750°C for around 20 minutes) in a nitrogen atmosphere. In this case, a high yield of N-GQDs is synthesized, with an atomic nitrogen doping rate of around 10% with respect to the carbon atoms (Figure 1.42).

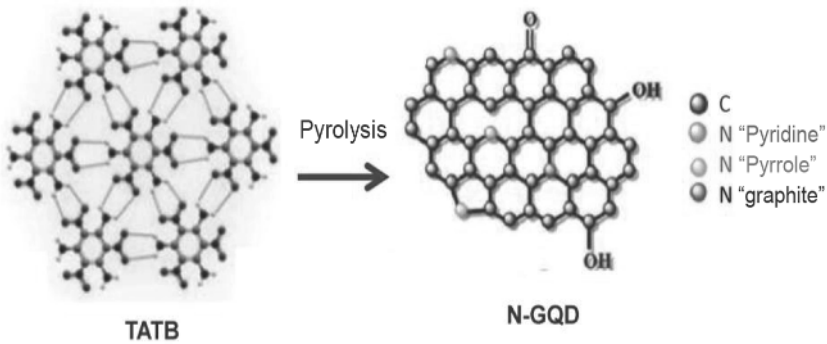

Figure 1.42. *N-GQD production by TATB pyrolysis*

COMMENT ON FIGURE 1.42.– *The TATB precursor is made up of a supramolecular planar network of TATB molecules linked by hydrogen bonds between the H in the NH_2 and the O in the NO_2 (the red, blue and gray spheres represent the oxygen, nitrogen and carbon atoms, respectively; the gray points in TATB are H atoms). Note that in N-GQD, the nitrogen atoms are incorporated into the graphitic network and occupy distinct positions corresponding to functionalities of different types (pyridine, pyrrole or graphite). Adapted from [LI 16c].*

The TATB precursor compound is already a bidimensional planar network with hexagonal symmetry. The neighboring TATB molecules are linked by intermolecular hydrogen bonds between NH_2 and NO_2. This supramolecular organization prefigures a graphene-like structure, likely facilitating the formation of N-GQDs.

This heteroatom doping technique has been widely applied to other atoms (boron, sulfur, phosphorus, halogens, alkali metals, etc.) using a wide variety of precursor systems, documented in an article by Tian *et al.* [TIA 18]. Simultaneous doping with two or more heteroatoms is also possible, and in this case, it is possible to produce GQDs with multiple emissions [QU 15].

1.6.2. *Properties and applications of GQDs*

Unlike graphene, GQDs have a non-zero energy band gap, the width of which depends on the size, shape and edge effects of the NPs. Considering the wide variety of methods used to produce GQDs and the wide range of possible sizes and shapes, it is not surprising that their optoelectronic and photoemission properties also vary widely. Photoemission is a key property in GQDs, and is used in various detection systems, with important applications in medical imaging.

1.6.2.1. *Photoluminescence properties of GQDs*

The photoluminescence of GQDs is determined both by the core of the nano-material, which may be assimilated to a graphene fragment, and by the surface states corresponding to functional groups positioned at the periphery of the NPs, along with the heteroatoms produced in the case of doping (Figure 1.43).

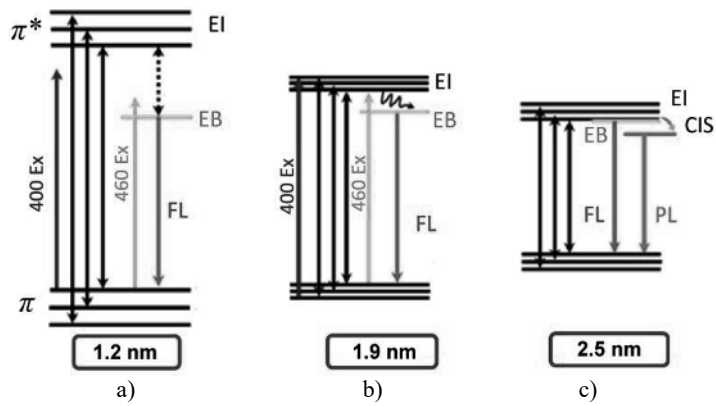

Figure 1.43. *Photoluminescence of GQDs, interpreted as a function of size and light excitation energy*

COMMENT ON FIGURE 1.43.– *a) GQD ($C_{42}H_{18}$, size 1.2 nm): fluorescent emissions (FL) are only obtained with excitation at 460 nm. b) GQD ($C_{96}H_{30}$, size 1.9 nm): a-intensity fluorescence emission is observed following excitations at 400 and 460 nm, resulting from an energy transfer from the intrinsic state EI (π*) to the edge state EB (trap level, due to the functional groups located on the periphery of the GQDs). c) GQD ($C_{132}H_{34}$, size 2.5 nm): the EB and EI states have the same energy, and there is a possibility of an intersystem crossing (ISC) between the intrinsic state and triplet state, resulting in simultaneous emissions of fluorescence (FL) and phosphorescence (PL). Adapted from [ZHU 14b].*

In a highly detailed spectroscopic study (both static and dynamic), Zhu *et al.* [ZHU 14b] showed that the photoemission properties of GQDs are determined by the energy level offset between the intrinsic state and the edge state in the GQD. The intrinsic state energy (EI) corresponds to the π* orbitals of graphene fragments, and the edge state energy (EB) corresponds to chemical edge groups, grafted onto the periphery of the GQD, which can be assimilated to energy traps.

Using GQDs of increasing size ($C_{42}H_{18}$-1.2 nm, $C_{96}H_{30}$-1.9 nm, $C_{132}H_{34}$-2.5 nm), the authors clearly show that the energy of the intrinsic π→π* transition decreases with the size of the GQD, along with the energy difference ΔE between the intrinsic states (π*) and edge states (EB). It is this energy difference ΔE that determines the nature and intensity of the luminescence originating from the deactivation of the edge states. The emission is essentially of the fluorescent type for non-zero ΔE, but this may be combined with phosphorescence when ΔE is zero. The fluorescence intensity may be very low, or even non-existent, when the energy level of the intrinsic state is close to that of the edge state; this is the case for GQDs of formula $C_{132}H_{34}$ and $C_{222}H_{42}$ [ZHU 14b].

A similar approach may also be used to describe the photoluminescence properties of GQDs which have been doped using different O and N heteroatoms in various proportions. In this case, the Jablonski diagram includes a n→π* transition in addition to the π→π* transition.

Qu *et al.* [QU 15] observed that nitrogen-doped GQDs of increasing sizes can produce blue (B), green (G) or yellow (Y) fluorescence, determined by the relative position of the n, π* and edge state energy levels[31]. The energy levels of these GQDs, named N-GQD-B, N-GQD-G and N-GQD-Y, respectively, are shown in Figure 1.44, and clearly illustrate the changes in fluorescence colors, which correlate with slight increases in GQD size corresponding to redshifts of the π→π*

31 The different N-GQDs are obtained by treating a mixture of citric acid and diethylene triamine (DETA) in an aqueous medium or N,N dimethyl formamide (DMF), resulting in different C/N and C/O ratios, which determine the fluorescence.

transitions. Compared to undoped GQDs of identical sizes, we note the presence of a red shift in fluorescence emissions. This is due to the fact that the electronic transition responsible for fluorescence occurs between the edge state and the non-bonding n-orbitals of the heteroatoms (O, N), rather than between the edge state and the lower energy π-orbital.

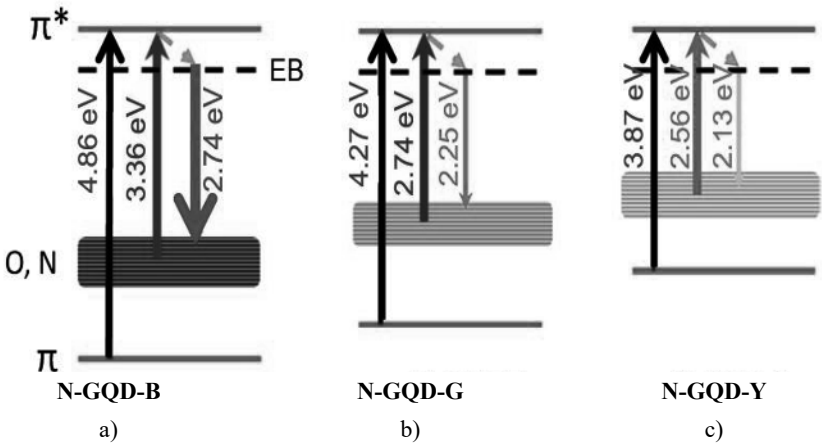

Figure 1.44. *Perrin-Jablonski diagrams of nitrogen and oxygen doped GQDs characterized by blue (B), green (V) and yellow (J) fluorescence*

COMMENT ON FIGURE 1.44.– *Energy diagrams a, b and c are deduced from the excitation and fluorescence spectra of different GQDs. Each of the compounds is characterized by two excitation bands π→π* and n→π* accompanied by a fluorescence emission band corresponding to the EB→n transition, resulting from a prior transition from π* to the EB state. The different energy values are deduced from the maxima of the excitation and emission bands of the corresponding spectra of the different GQDs. The values of 2.74 eV, 2.25 eV and 2.13 eV correspond, respectively, to blue (450 nm), green (550 nm) and yellow (580 nm) light emissions. Adapted from [QU 15].*

1.6.2.2. *Applications of GQDs*

A significant body of work has been produced over the last few years focusing on potential uses of GQDs for energy and biomedical applications. In the energy field, GQDs offer the potential for important improvements in battery electrode performance and in supercapacitor performance. Their photoluminescence properties have also been used to improve the operation of OLEDs and photovoltaic devices; furthermore, GQDs also have a positive contribution to make to photocatalytic processes. The largest number of potential applications,

however, is found in the biomedical field; GQDs may be used in applications as varied as imaging and drug delivery, various forms of phototherapy, and in the production of antibacterial products. We have chosen to limit our discussion to a few examples of applications in photodetection devices, used in trace analysis or to detect radiation; in these contexts, GQDs are often used in the form of composite materials.

1.6.2.2.1. Use of GQD composites for detecting volatile organic compounds

Certain devices used to detect gases or volatile organic compounds (VOCs) at low concentrations make use of the variations in the conductivity of a solid film which occur in contact with a gas. Conductive polymers such as polypyrrole and PEDOT (poly[3,4-ethylenedioxythiophene]) exhibit observable variations in conductivity when interacting with volatile compounds. Graphene, and more recently GQDs, has been suggested as additives for these films, allowing an increase in sensitivity and in the specificity of VOC detection.

A device of this type has been made using a nanocomposite consisting of N-GQD and poly(3,4-ethylenedioxythiophene)-poly(styrenesulfonate) (PEDOT-PSS). The N-GQD/PEDOT-PSS mixture took the form of a suspension in a water-dimethyl sulfoxide medium (10 wt% DMSO); the classic hydrothermal method of transforming of a mixture of citric acid and urea was used to create the N-GQDs (diameter between 2 and 7 nm, atomic ratio N/C equal to 0.058). One drop of the previous mixture was deposited on a flat surface with interdigitated gold electrodes, arranged according to conventional lithography techniques, then the whole assembly was annealed at 80°C. This had the effect of covering the interdigitated electrode area with a N-GQD/ PEDOT-PSS film. The contacts are two conductive wires connected to the gold electrodes with silver solder (Figure 1.45).

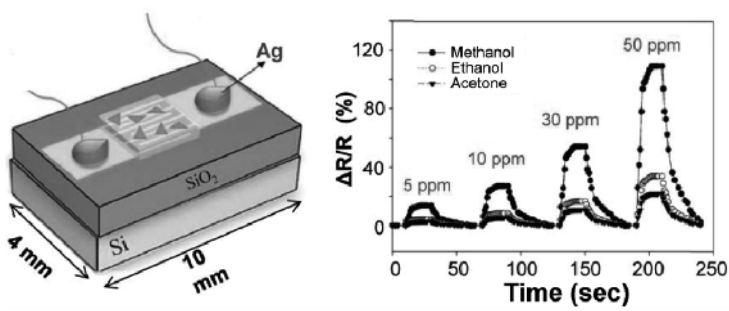

a) b)

Figure 1.45. *VOC detection device, using variations in the resistance of a N-GQD/PEDOT-PSS film*

COMMENT ON FIGURE 1.45.– *a) View of the device showing the area of interdigitated gold electrodes covered by nanocomposite film. The interdigitated gold electrodes are 100 nm thick; their width is 200 µm and their spacing is 400 µm. b) Relative changes in the resistance of the composite film subjected to different concentrations in air (5, 10, 30 and 50 ppm) of methanol, ethanol and acetone vapor. Adapted from [GAV 15].*

When in contact with methanol, ethanol and acetone vapors, the resistance of the film, measured between the two contacts, increases as a function of VOC concentration. The relative change in resistance (ΔR/R) is nearly linear between 0 and 50 ppm concentration, after which the system is saturated and the resistance no longer depends on concentration. Note that the response time is of the order of 10 seconds; the return to equilibrium, while slightly slower, is of the same order of magnitude.

The presence of N-GQDs in the composite is necessary for a strong increase in resistance to be observed in the presence of different VOCs. The resistance of a film made up of N-GQDs alone hardly varies in contact with these vapors, while in the case of a film composed only of PEDOT-PSS, the relative variation in resistance does not exceed 10%. With N-GQDs as additives, the relative variation in R is 130%. Moreover, the response is noticeably greater in the presence of methanol than with ethanol and acetone: this must be attributed to the stronger reducing character of methanol, which partially reduces the PEDOT and thus increases its resistivity. The return to equilibrium occurs due to the oxygen in the air, which re-establishes the initial oxidation state of the PEDOT and thus its original conductivity.

Paradoxically, methanol only has a weak effect on a PEDOT:PSS film alone and almost none on a film composed only of N-GQDs, but when the two are combined, a considerable variation in resistance is observed. The authors attribute this difference in behavior to the fact that (i) the initial σ-conductivity of PEDOT:PSS is greatly increased by the presence of N-GQDs ($\sigma_{PEDOT:PSS}$ = 635 S/cm and $\sigma_{N\text{-}GQD/PEDOT:PSS}$ = 1365 S/cm) and (ii) the initially compact PEDOT:PSS film becomes porous in the presence of N-GQDs, allowing increased diffusion of VOCs inside the film and thus a greater reduction of the PEDOT, resulting in increased resistance.

1.6.2.2.2. Photodetectors for UV radiation

Conventional UV detectors are fabricated from wide band gap inorganic semiconductor films, such as ZnO, GaN, AlGaN or Si, but these may be replaced by GQDs; this latter option presents the advantage of being easy to obtain in solution,

which results in clear benefits in terms of both design and cost. Unlike graphene, which has a zero energy band gap, the energy band gap of GQDs can be easily tuned to be compatible with UV absorption energies: this is done by reducing their size to that of 0 dimensional (0D) NPs.

Zhang *et al.* [ZHA 15] have designed a UV photodetector in which the sensor layer of the device (80 nm thick) is made of GQDs sized between 2.5 and 6 nm with a thickness equivalent to 1 and 4 graphene layers (from 0.4 to 2.5 nm)[32]. The band gap, measured by electrochemistry, is equal to 3.6 eV.

The principle used to detect luminous radiation is a classic one, and consists of measuring, for a voltage applied between two electrodes, the electric current resulting from the creation of an electron-hole pair in the semiconductor under the effect of the irradiation (metal/GQD/metal junction). The authors showed that the highest sensitivity was obtained in the case of an Au/GQD/Ag junction in which a voltage of 5 volts is applied between the electrodes and where the gold electrode is positively polarized. This configuration has the effect of making the Au/GQD (+) and Ag/GQD (–) contacts ohmic: one for the transfer of electrons, the other for the transfer of holes. The device is sensitive to UV radiation of wavelengths below 300 nm and insensitive to white light (Figure 1.46).

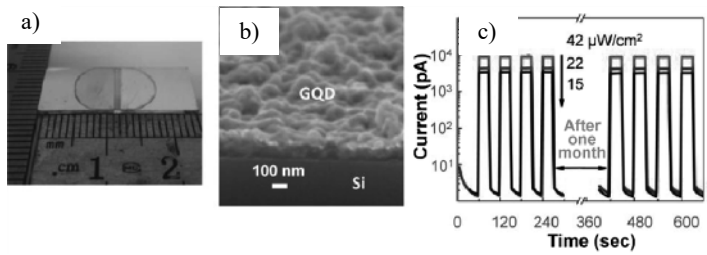

Figure 1.46. *UV detection device. a) Photograph of the Au/GQD/Ag junction. b) SEM image of the GQD film covering the channel between the two electrodes. c) Variations of the photocurrent subjected to UV light pulses at 342 nm of different intensities (42, 22 and 15 µW/cm^2). Note the high stability of the device after one month. Adapted from [ZHA 15]*

32 The GQDs are synthesized from graphene sheets (GS) obtained by deoxygenation (300°C under nitrogen atmosphere) of graphene oxide (GO). The GS are then oxidized in a mixture of sulfuric acid and nitric acid under ultrasonic agitation, diluted in water, and then filtered to obtain a first purified suspension of oxidized GS. A final autoclave treatment of the suspension at 200°C (10 h) and filtration results in the obtention of GQDs.

1.6.3. *Graphdiyne: a new alternative to graphene*

A new family of 2D carbon-based compounds, known as graphynes, was first identified in the 1980s by Baughman and Eckhardt [BAU 87]. Graphynes are graphene-derived compound planes, in which the benzene rings are covalently linked by n conjugated –C≡C– ethyne groups instead of being fused together (Figure 1.47).

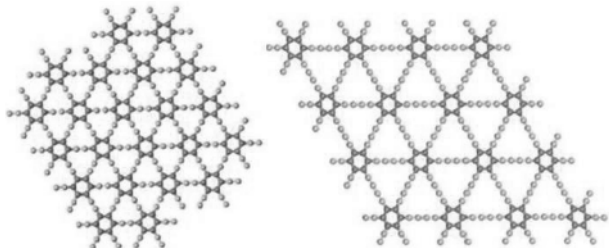

a) b)

Figure 1.47. *Diagrammatic representation of graphynes. a) Simple graphyne (n = 1) in which the benzene rings (shown in blue) are linked, at their vertices, by acetylenic groups –C≡C– (in pink). b) Structure of graphdiyne: this differs from the previous example in that the simple –C≡C– bonds have been replaced by diethynyl groups –C≡C–C≡C– (n = 2). Adapted from [LIU 17a]*

These ethyne groups form rigid linear links between benzene rings, resulting in the formation of planar and porous networks of sp and sp^2 hybridized carbons. These compounds are named graphyne-1, graphyne-2, graphyne-3, etc., according to the number (n) of ethyne groups linking the vertices of the benzene rings. Like graphene, these compounds are mechanically robust; however, their calculated rigidity characteristics are lower than those of graphene, and decrease when the number of ethynyl groups increases.

Graphyne-2 (or graphdiyne, GDY) is the most stable and, at present, the only graphyne to have been synthesized in appreciable quantities. This synthesis was carried out by Yuliang Li [LI 10a] and colleagues in 2010; since then, many works have been published on the subject of GDY from both theoretical and experimental perspectives. This interest is justified by the remarkable structural, electronic, mechanical and thermal properties of the material, which suggest new potential applications, notably in the fields of energy, catalysis and in the design of systems based on the photoelectronic conversion principle [GE 19, KAN 19a].

The formation reaction described by Li *et al.*, used to obtain GDY in large quantities and with good yields, consists of reacting hexaethynylbenzene (HEB) on a copper substrate in the presence of pyridine and in a nitrogen atmosphere at a

temperature of 60°C [LI 10a]. This produces a large-area homogeneous film, consisting of multiple layers of GDY with a total thickness of about 1 μm. Since then, other variants of the method have been proposed, notably the deposition of GDY films on different solid substrates (Si, Ag and Au) as well as on graphene sheets.

Generally speaking, most of these methods use the same HEB precursor; the details of these reactions are described in detail by Gao *et al.* [GAO 19]. As for other carbon-based materials, GDY can also be doped with heteroatoms; this has been demonstrated using nitrogen, and also with simultaneous insertion of two elements such as F and N, S and N or B and N. These may substitute or link to the sp carbons in the ethynyl bonds, resulting in GDY with new catalytic properties. The material obtained by doping GDY with F and N, for example, is an excellent catalyst for the electrochemical reduction of oxygen in a basic medium [ZHA 16a].

It is significant that GDY can be produced without the use of high temperatures, unlike graphene and its derivatives; this is an additional advantage when considering possible large-scale applications.

1.6.3.1. *Properties of graphdiyne*

The presence of diethynyl bonds between benzene rings results in new properties which are not found in the condensed structure of graphene, paving the way for new applications.

In terms of electronic properties, there are notable similarities to graphene, particularly with regard to the mobility of charge carriers. Their calculated mobility is very high, between 10^4 $cm^2/Vsec$ for holes and 10^5 $cm^2/Vsec$ for electrons; this latter value is of the same order of magnitude as that observed for graphene, for which the mobilities of electrons and holes have been estimated at 3×10^5 $cm^2/Vsec$ (theoretical) and measured at between 2 and 25×10^4 $cm^2/Vsec$ [CHE 13a].

However, GDY differs from metal graphene in terms of its low-gap semiconductor properties, evaluated according to different methods at between 0.46 and 1.10 eV for single-layer GDY. Unlike graphene, GDY thus has the potential to be used in creating various electronic devices in which organic transistors are used. The conductivity of a multilayer GDY film of 1 μm thickness, synthesized on a copper substrate, is around 2.5×10^{-2} S/cm; this value is comparable to that of silicon [LI 10a]. In the case of GDY wires produced using a different technique, much higher conductivities of 1.9×10^5 S/cm have been measured, but in this case the mobility value is lower, around 7×10^2 $cm^2/Vsec$. The authors attribute this difference in conductivity between films and wires to the absence of defects in the process used to produce GDY wires [QIA 12b].

The presence of calibrated triangular pores (with an approximate size of 2.5 Å) [HAL 08] is another notable difference between GDY and graphene, offering perspectives for further applications, notably in selective membranes for gas separation. Another important property of GDY is the possibility of inserting metals in the atomic state, which can be used, for example, to produce electrodes. Furthermore, this property can be used in fuel cells to improve the electrochemical reactions of oxygen reduction or proton reduction in an acidic medium (see Chapter 5, "Electro and photo-electrocatalysis").

These characteristics of GDY make it suitable for use in a wide variety of applications, a comprehensive list of which can be found in Gao *et al.* [GAO 19] and Yu *et al.* [YU 19]. Notable potential applications for GDY include use as a membrane for the separation of gases (H_2, O_2 and N_2), a functional role as a catalyst support in the atomic state (see Chapter 5, section 5.3.1), and significant improvements to electrode function in lithium-ion batteries (LIBs).

1.6.3.2. *Some specific applications of graphdiyne*

The porosity and electronic conductivity GDY mean that it has great potential for use in electrode manufacture. These electrodes may be used in batteries, or as catalysts for the reduction of oxygen and protons in fuel cells. Two examples of GDY use in these fields are described below.

1.6.3.2.1. Catalysts for oxygen reduction reaction

One important objective in the development of fuel cells with an oxygen cathode is to replace the excellent, but very expensive, platinum or platinum/carbon electrodes with catalytic systems based on low-cost non-noble metals.

GDY has been doped with heteroelements with the aim of developing efficient electrodes, likely to improve the kinetics of the oxygen reduction reaction (ORR). Doping with nitrogen and fluorine produces an NF-GDY material with a high catalytic power for the ORR, comparable to that of C/Pt electrodes (20 wt% Pt) [ZHA 16a], and much higher than that of electrodes consisting of GDY alone or GDY doped with N and S (NS-GDY), or N and B (NB-GDY) (Figure 1.48).

Doping is carried out by reacting GDY powder first with NH_4F and then with NH_3 at high temperatures (700°C). This reaction increases the number of structural defects in the initial GDY, resulting in greater porosity. The increase in porosity is due to the fact that fluorine binds preferentially to sp carbons, leading to the bonds between a benzene ring and an ethynyl bond breaking down. Nitrogen atoms, on the

other hand, can either take the place of sp^2 carbons in the benzene rings or bind to sp carbons[33].

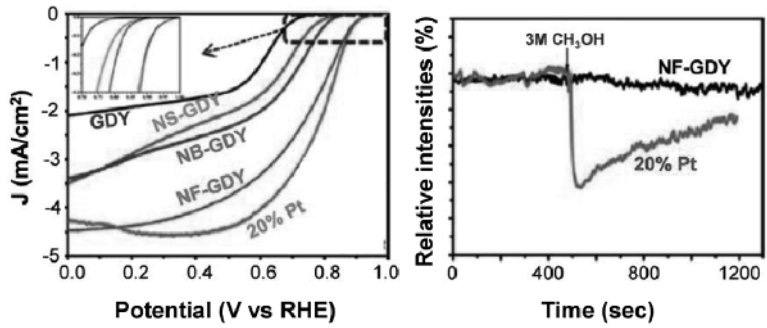

a) b)

Figure 1.48. *Electrochemical reduction of O_2 on GDY electrodes doped with different elements in an alkaline medium (0.1 M KOH solution saturated with O_2) in comparison with a Pt/C electrode*

COMMENT ON FIGURE 1.48.– *a) J/V curves obtained using a linear voltage sweep (10 mV/sec). b) An addition of 3 M CH_3OH to the oxygen-saturated solution has no effect on the behavior of the NF-GDY electrode, in contrast to the Pt electrode, which exhibits a significant drop in the oxygen reduction rate. Adapted from [ZHA 16a].*

The electrocatalytic properties of NF-GDY electrodes, evaluated by electrochemical reduction of an O_2-saturated solution in an alkaline medium, are comparable to those of a Pt composite surface made up of a classic C/Pt mixture. Moreover, contrary to Pt, the behavior of the NF-GDY electrode is little affected by the presence of CO or methanol, often indicated as the reason for a loss of efficiency in Pt electrodes.

In short, with regard to oxygen reduction, N and F-doped GDY has electrochemical characteristics that are comparable to those of commercial Pt/C composite electrodes. The presence of N and F appears to be decisive in this respect. Comparable effects have also been demonstrated with mesoporous graphene electrodes doped with N and F heteroatoms [ZHA 16a].

33 This multiplication of the number of defects in the GDY structure is illustrated by Raman spectroscopy, and can be seen in the ratio of the I_D/I_G intensities of the two characteristic bands D and G located at 1350 cm^{-1} and 1620 cm^{-1}, respectively. The number of defects increases as the I_D/I_G ratio increases.

1.6.3.3. *Use of a modified GDY structure as a super-cathode in Lithium-ion batteries*

The presence of channels running perpendicular to the GDY plane constitutes an improvement in comparison with graphite, allowing ions such as Li^+ to penetrate more easily into the planes. The fact that the interior of the vacancies may be modified with chemical groups which have the capacity to stabilize these ions is a further improvement, developed recently by Li and coworkers [WAN 17].

They aimed at synthesizing a chlorinated hexadiethynyl benzene (HEB) monomer, such as 1,3,5-(triethynyl-2,4,6-trichlorobenzene), in which chlorine atoms alternate with ethynyl groups (Figure 1.49a) [WAN 17]. This monomer can be polymerized under the same conditions as HEB, resulting in a chlorinated GDY compound (Cl-GDY) (Figure 1.49b). The resulting product displays larger pores (1.6 nm), which are hexagonal in shape, rather than triangular as in the case of GDY, for which vacancies are around 0.25 nm in size [HAL 08]. This larger pore size enables the insertion of a greater quantity of alkaline atoms and facilitates their diffusion inside Cl-GDY; the moderate electronegative character of the chlorine atoms which are uniformly distributed throughout the Cl-GDY contributes to stabilizing the implantation of these alkaline ions.

This material, deposited as a thick film of about 2.8 μm on a metallic copper substrate (Cu/Cl-GDY), was used by the authors to build a cell using a Li film as the anode and the Cu/Cl-GDY electrode as the cathode[34].

The charge/discharge curves between 0.005 and 3 V show Li^+ ion storage capacities which are much higher than those obtained using GDY alone. For current densities of 50 mA/g, the Li^+ storage capacities are 1150 mAh/g; a value of 500 mAh/g was obtained for charge/discharge rates (C/D) of 2 A/g (Figure 1.49c). In the case of a GDY electrode, the storage capacity is only 450 mAh/g for C/D rates of 100 mA/g[35] .

These results confirm the stabilizing role of chlorine atoms with respect to Li^+ ions. In addition, the larger pore size of Cl-GDY compared to GDY is likely to result in the storage of larger amounts of Li^+.

---

34 The conductivity of the Cl-GDY film, which is higher than that of GDY ($2.5.10^{-4}$ S/m), is around 2.10^{-3} S/m. The two electrodes are separated by a polypropylene film. The electrolytic solution is a classic mixture of organic solvents (dimethyl carbonate and ethylene carbonate in equal volumes) with the addition of $LiPF_6$ (1M).

35 For most current lithium-ion batteries, the specific capacities of the lithium insertion cathodes do not exceed 250 mAh/g [GUO 17b].

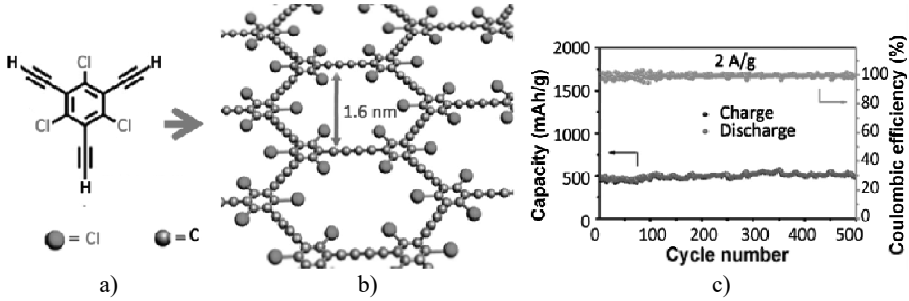

Figure 1.49. *Production of Cl-GDY and lithium-ion storage capacities*

COMMENT ON FIGURE 1.49.– *a) Structure of the monomer used to obtain Cl-GDY. b) Structure of the chlorinated derivative: Cl-GDY. c) Charge-discharge curves for Li^+ ions at high current intensity (2 A/g) with a Cl-GDY electrode. Note that the charge and discharge capacities (of the order of 500 mAh/g) are nearly equal to one another (corresponding to 100% coulombic efficiency), with no noticeable change after 500 charge/discharge cycles. Adapted from [WAN 17].*

1.7. Conclusions and perspectives of carbon-based nanomaterials

Over the last 20 years, new families of carbon-based nanomaterials have emerged. These materials present striking new properties and have the potential to be used in a wide range of applications, solving problems encountered in the fields of energy, electronics and biology. Given two materials with similar properties, preference will be given to that which is easiest to produce on a large scale and at reasonable cost: essential considerations for any potential industrial or commercial application.

Fullerenes and CNTs (some of the oldest materials discussed here), graphene and their derivatives take center stage; surprisingly, given a basic structure based solely on carbon chains in sp^2 hybridization, these materials present very clearly differentiated properties according to their dimensional characteristics: 0D for fullerenes, 1D for CNTs and 2D for graphene and GDY. The first three of these materials are now commercially available, a fact which is explained by their range of uses in crucial areas of application. Certain fullerenes, such as a C_{70} derivative, have been used to improve the energy yields of photovoltaic cells; CNT, graphene and their functionalized derivatives have been particularly successful because of their exceptional electrical and mechanical properties, which allow them to be used in new hybrid plastic materials with improved mechanical and electrical properties.

As we shall see later, these materials have also been used in the production of composite electrodes for electrocatalysis, energy storage and conversion applications.

Currently, the largest number of actual and potential applications has been found for graphene and its derivatives (GO); these take the form of plasticized tapes, foams, papers or fibers, which combine both excellent electrical and mechanical properties. Graphene fragments of nanometric dimensions – GQDs – present remarkable fluorescence properties and are characterized by non-zero energy band gaps, allowing their use in constructing various optoelectronic devices.

Most of these nanomaterials compete with activated carbons for applications in the field of electrochemistry, notably in the design of capacitive devices. In many cases, their cost is significantly higher than that of activated carbons, meaning that their use is only justified if a small quantity of product can be used to offer a significant improvement in terms of properties.

Nanodiamonds (ND), carbon NPs in the form of CQD, constitute a further family of these new materials. NDs are distinguished by their small size – less than 10 nm – and by different types of carbon-carbon bonds involving variable proportions of sp^2 and sp^3 hybridizations. NDs feature a majority of bonds between sp^3 carbons; in CQDs, the core of the particle is essentially made up of graphitic-type sp^2 carbons. These materials are commercially available, and are much easier to obtain than fullerenes, CNTs and graphene, which also makes them cheaper. For some electrochemical applications (energy storage and electrolytic capacitors), CQDs are now in a position to compete with activated carbons. They are also characterized by fluorescent properties which clearly differentiate them from fullerenes, CNT and graphenes, which are intrinsically non-luminescent. Moreover, the presence of hydrophilic functional groups on the surface means that these particles are soluble in aqueous media and, due to their non-toxicity, they are excellent candidates for use in medical imaging.

Research into new and improved methods for producing carbon nanomaterials, and on developing uses for these materials in a wide variety of fields, continues to progress. New carbon nanomaterials, such as GDY – which is a semiconductor – are also emerging. GDY possesses remarkable properties including controlled porosity and the ability to adsorb elements in the atomic state, properties which open new perspectives for uses in catalysis, for example. Described as a “rising star”, GDY looks set to take its place as an important member in the family of 2D semiconductors in the near future.